Remote Sensing of Environment 182 (2016) 192–207

Contents lists available at ScienceDirect

Remote Sensing of Environment

journal homepage: www.elsevier.com/locate/rse

Mapping changing distributions of dominant species in oil-contaminated salt marshes of Louisiana using imaging spectroscopy

Michael Beland [a,b,*], Dar A. Roberts [b], Seth H. Peterson [b], Trent W. Biggs [a], Raymond F. Kokaly [c], Sarai Piazza [d], Keely L. Roth [e], Shruti Khanna [e], Susan L. Ustin [e]

[a] Department of Geography, San Diego State University, CA 92182, USA
[b] Department of Geography, University of California, Santa Barbara, CA 93106, USA
[c] U.S. Geological Survey, MS 973, Box 25046, Denver, CO 80225, USA
[d] U.S. Geological Survey, C/O Livestock Show Office, Parker Coliseum, Baton Rouge, LA 70803, USA
[e] Department of Land, Air, and Water Resources, University of California, Davis, Davis, CA 95616, USA

ARTICLE INFO

Article history:
Received 16 September 2015
Received in revised form 17 March 2016
Accepted 30 April 2016
Available online 31 May 2016

Keywords:
AVIRIS
Deepwater Horizon
Oil spills
Image classification
Dominant species mapping
Salt marsh vegetation
Canonical discriminant analysis
Hyperspectral remote sensing

ABSTRACT

The April 2010 Deepwater Horizon (DWH) oil spill was the largest coastal spill in U.S. history. Monitoring subsequent change in marsh plant community distributions is critical to assess ecosystem impacts and to establish future coastal management priorities. Strategically deployed airborne imaging spectrometers, like the Airborne Visible/Infrared Imaging Spectrometer (AVIRIS), offer the spectral and spatial resolution needed to differentiate plant species. However, obtaining satisfactory and consistent classification accuracies over time is a major challenge, particularly in dynamic intertidal landscapes.

Here, we develop and evaluate an image classification system for a time series of AVIRIS data for mapping dominant species in a heavily oiled salt marsh ecosystem. Using field-referenced image endmembers and canonical discriminant analysis (CDA), we classified 21 AVIRIS images acquired during the fall of 2010, 2011 and 2012. Classification results were evaluated using ground surveys that were conducted contemporaneously to AVIRIS collection dates. We analyzed changes in dominant species cover from 2010 to 2012 for oiled and non-oiled shorelines.

CDA discriminated dominant species with a high level of accuracy (overall accuracy = 82%, kappa = 0.78) and consistency over three imaging dates ($overall_{2010}$ = 82%, $overall_{2011}$ = 82%, $overall_{2012}$ = 88%). Marshes dominated by *Spartina alterniflora* were the most spatially abundant in shoreline zones (≤28 m from shore) for all three dates (2010 = 79%, 2011 = 61%, 2012 = 63%), followed by *Juncus roemerianus* (2010 = 11%, 2011 = 19%, 2012 = 17%) and *Distichlis spicata* (2010 = 4%, 2011 = 10%, 2012 = 7%).

Marshes that were heavily contaminated with oil exhibited variable responses from 2010 to 2012. Marsh vegetation classes converted to a subtidal, open water class along oiled and non-oiled shorelines that were similarly situated in the landscape. However, marsh loss along oil-contaminated shorelines doubled that of non-oiled shorelines. Only *S. alterniflora* dominated marshes were extensively degraded, losing 15% (354,604 m^2) cover in oiled shoreline zones, suggesting that *S. alterniflora* marshes may be more vulnerable to shoreline erosion following hydrocarbon stress, due to their landscape position.

1. Introduction

Coastal wetlands of the Gulf of Mexico provide a wide range of vital ecosystem services, including storm surge protection, water quality enhancements, carbon sequestration, wildlife habitat, fisheries and recreational opportunities (Mitsch and Gosselink, 2000; Reddy and DeLaune, 2008). However, for nearly two centuries, the states around the northern Gulf of Mexico have experienced elevated rates of intertidal wetland loss (>250 km^2 yr^{-1}: Stedman and Dahl, 2008), due to a combination of natural disturbances (e.g. hurricanes, tropical storms), and anthropogenic activities (e.g. wetland drainage, canal dredging, river channelization and reduced sediment loads from the Mississippi River). Louisiana alone lost an estimated 4800 km^2 of intertidal wetland area from 1932 to 2010 (~62 km^2 yr^{-1}: Couvillion et al., 2011).

On April 20, 2010, an explosion occurred on the Deepwater Horizon (DWH) offshore drilling unit at the Macondo well about 64 km off the coast of Louisiana. An estimated 780,000 m^3 of crude oil was released into the Gulf before the well was successfully capped on July 15, 2010 (Lehr et al., 2010). Oil washed onto shorelines of several Gulf States, including approximately 796 km of Louisiana shoreline composed of

* Corresponding author at: Department of Geography, San Diego State University, CA 92182, USA.
E-mail address: mbeland@rohan.sdsu.edu (M. Beland).

http://dx.doi.org/10.1016/j.rse.2016.04.024
0034-4257/

intertidal marshes (Michel et al., 2013). Past incidences of oiling have shown that marsh recovery trajectories can vary greatly, from temporary reductions in stomatal conductance and photosynthetic rates (Pezeshki and De Laune, 1993) to plant mortality, substrate destabilization and marsh shoreline erosion (Lin and Mendelssohn, 1996; Lin and Mendelssohn, 2012). The long-term effects of an oil spill of this magnitude on marsh ecosystems remain unknown due to variations in exposure properties (Alexander and Webb, 1985; Pezeshki et al., 2000), landscape characteristics, such as marsh surface elevation (Hester and Mendelssohn, 2000), distance to shoreline (Khanna et al. 2013) or exposure to wave action (Silliman et al., 2012) and plant community composition (Pezeshki and De Laune, 1993; Lin and Mendelssohn, 1996; Lin and Mendelssohn, 2012).

Studies conducted after the DWH spill suggest that oil coverage extended <15 m inland from the seaward edge of marshes (Silliman et al., 2012), reaching a maximum of 21 m (Kokaly et al., 2013), and vegetation stress was largely restricted to the zone extending 14 m from the shoreline (Khanna et al., 2013). Lin and Mendelssohn's (2012) findings indicate that impacts to salt marsh plant communities were variable depending upon oiling intensity, and suggested that the locations most impacted by oiling were dominated by *Spartina alterniflora* and *Juncus roemerianus*. However, the distribution of plant communities that were impacted, and the degree of community change have not been quantitatively determined.

Dominant species shape community structure and are a useful indicator of plant community condition (Frieswyk et al., 2007). More specifically, identifying dominant species and changes in spatial distribution can help explain long-term marsh ecosystem responses to oil (Lin and Mendelssohn, 1996; DeLaune et al., 2003). Most crude oils are nonionic, and associate more readily with organic particles (Pezeshki et al., 2000). Consequently, soil organic matter (SOM) in a marsh substrate impacts the persistence of oil residues, and SOM content in turn varies with plant species composition (Lin and Mendelssohn, 1996). In a comparative greenhouse study, Lin and Mendelssohn (1996) reported both higher SOM content and higher oil residual concentrations in plots dominated by *Spartina patens* than in plots dominated by *S. alterniflora*. Additionally, *S. alterniflora* has exhibited a greater recovery rate than other common dominant marsh species (e.g. *Distichlis spicata*, *S. patens* and *J. roemerianus*) in field experiments, indicating a higher tolerance threshold for oil contamination (Mendelssohn et al., 1990; Lin and Mendelssohn, 2012).

Accordingly, mapping community dominants and changes in distribution are valuable components of ecosystem assessments. Yet, quantitative assessments of plant community impacts are infeasible using field-based methods, due to the large size of the DWH oil-affected area. Remote sensing has become an attractive tool for evaluating responses of vegetation to disturbance and for "scaling up" in situ observations to landscape scales, due to the relatively high cost and time requirements of traditional field assessments and the inaccessibility of many areas. More recently, narrow-band, hyperspectral sensors, like the Airborne Visible/Infrared Imaging Spectrometer (AVIRIS), have produced images with fine enough spectral resolution (~10 nm) to discriminate ground constituents that were previously indistinguishable with broadband sensors. As a result, increasingly sophisticated image classifiers, feature extraction and spectral unmixing algorithms have been developed to derive more detailed information from spectroscopic data, including pigment (Demmig-Adams and Adams, 1996; Gamon et al., 1997; Feret et al., 2008; Ustin et al., 2009), non-pigment (Ceccato et al., 2001; Asner et al., 2003; Serrano et al., 2002; Nagler et al., 2003; Kokaly et al., 2009) and biochemical constituents of vegetation (Asner, 1998).

Species-level classification, however, remains a substantial challenge due to the spectral similarity of many species, particularly those within the same functional type (Ustin and Gamon, 2010; Roth et al., 2015), and spatial, temporal and spectral variability of a single species (Somers et al., 2009; *see* Somers et al., 2011, *for review of endmember variability*). Mapping coastal vegetation is further complicated by sharp environmental gradients, such as salinity and anaerobic stress, phenology, and the tidal regime, all of which enhance spectral variability over space and time (Schmidt and Skidmore, 2003; Adam et al., 2010).

Developing techniques that optimize the use of training data to minimize spectral variability within classes and reduce data dimensionality are active areas of remote sensing research as they may improve classification accuracies both spatially (Roth et al., 2015) and temporally (Peterson et al., 2015). A broad range of endmember optimization (Somers et al., 2011), dimension reduction (Dópido et al., 2012) and classification techniques (Lu and Weng, 2007) have been applied to hyperspectral images for vegetation mapping (Xie et al., 2008 *for review of vegetation mapping*), all of which have advantages and limitations that should be considered in relation to the analysis objectives, spatial and temporal factors, and landscape complexity (Lu and Weng, 2007). With high dimensional data, like AVIRIS, reducing the number of spectral bands used for classification is often necessary to retrieve satisfactory results, due to the redundancy and collinearity of some bands (Hughes, 1968), particularly those close in spectral distance. Canonical discriminant analysis (CDA) with a linear discriminant allocation rule has performed well in addressing class discrimination problems (Palacios-Orueta and Ustin, 1996; Guang and Maclean, 2000; Pu and Liu, 2011; Alonzo et al., 2013; Roth et al., 2015). CDA is a combined dimension reduction and classification method that transforms high-dimensional datasets into discriminant functions that maximize the difference ratios between class means and standard deviations. Subsequently, CDA selects variables with significant discriminating power, discarding unexplained noise and redundancy (Fisher, 1936; Guang and MacLean, 2000; Roth et al., 2015). As a result, CDA is well suited for distinguishing spectrally similar image constituents, such as perennial marsh grasses, because it removes spectral bands that are collinear (Plaza et al., 2009).

Field surveys have reported that Barataria Bay was among the most heavily impacted areas by oil following the DWH spill (Michel et al., 2013). Three recent studies have detected oil and mapped the extent of oil and persistence in Barataria Bay with greater detail using imaging spectroscopy (Khanna et al., 2013; Kokaly et al., 2013; Peterson et al., 2015). Kokaly et al. (2013) compared AVIRIS data with field-collected spectra of oiled marsh, focusing on the spectral absorption features related to the hydrocarbon (C—H) bond, to delineate the distribution of oiled marshes. Khanna et al. (2013) used a continuum removal technique centered on two oil absorption features to detect oil contamination on AVIRIS images. Peterson et al. (2015) used stable zone unmixing (SZU: Somers et al., 2010) and synthetic mixture analysis to determine which bands had discriminating power for oiled and non-oiled marshes. Nine bands (1-visible (685 nm), 4-short-wave infrared 1 (SWIR1, 1263, 1622, 1732, 1772 nm), and 4 SWIR2 (2038, 2208, 2238, 2277 nm)) effectively discriminated oiled marsh from live and dead vegetation (Peterson et al., 2015). Here, we used the approach from Peterson et al. (2015) to identify oiled zones, and applied CDA to all bands to map dominant species. We evaluated the suitability of time series imaging spectroscopy for mapping dominant species and for assessments of plant community distribution change after the spill. The following questions provide a framework for examining the suitability of the approach:

1. How well can spectrally similar salt marsh species be discriminated using airborne imaging spectroscopy? Do the maps of dominant species correspond to expectations based on expert knowledge of regional species distributions?

2. Which plant communities, defined by dominant species, were most affected by oiling, and how did the spatial distribution of those communities change?

3. How did marsh area conversion to open water compare between oiled and non-oiled shoreline reaches and for different dominant species?

S. alterniflora and *J. roemerianus* were the primary dominants inhabiting oil-contaminated marshes of Barataria Bay (Lin and Mendelssohn, 2012; Kokaly et al., 2013). No study has quantitatively or spatially documented the cover of these species or of other less common salt marsh dominants (e.g. *Phragmites australis*, *D. spicata*, and *S. patens*) in the impacted area. Further, no studies have documented

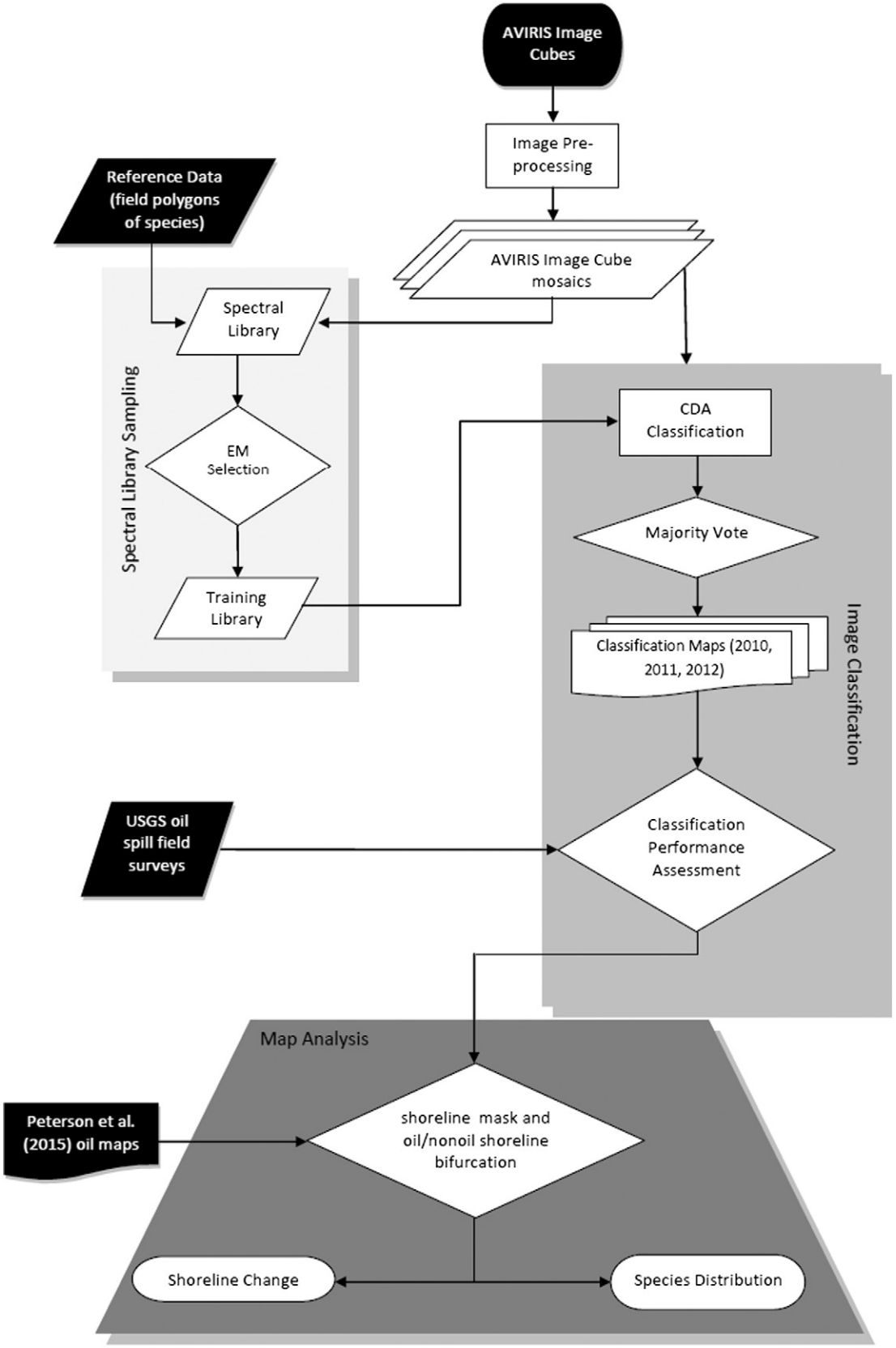

Fig. 1. Work flow schematic illustrating the AVIRIS and reference datasets (black boxes) image processing, spectral sampling, classification and map analysis methodology.

changes in the distribution of those dominants following the incident. Here, we devise an image classification scheme and examine the spatial distribution of salt marsh dominants on a landscape-scale, including *S. alterniflora*, *J. roemerianus*, *P. australis*, *D. spicata* and *S. patens* (Fig. 1). Finally, we evaluate the dominant species cover change in oiled and in adjacent, non-oiled zones for potential oil-related impacts to marsh community distributions, including conversion of marsh to open water.

2. Material and methods

2.1. Study area

Following the 2010 DWH spill, the most heavily oiled marsh shorelines were located in northern Barataria Bay, Louisiana (29.43°N, 89.88°W, approximately 60 km south of New Orleans) (Fig. 2B). The marsh ecosystems of this study area, which cover approximately 197 km^2, are typical of coastal wetlands throughout the Mississippi Delta region and are strongly influenced by the subtropical climate as well as by oceanic and fluvial processes. Salt marshes of Barataria Bay are fractions of a meter from sea level and are being impacted greatly by sea level rise (Penland and Ramsey, 1990). The vegetation types commonly found in the northern portion of Barataria Bay are characterized by low species richness (Visser et al., 1998). The common dominant species were identified using the 2007 Louisiana coastwide vegetation survey (Visser et al., 1998; Sasser et al., 2008). A dataset of >8000 records was queried to determine which dominant species were commonly observed at Braun-Blanquet cover-abundance category 6 levels (>75%: *see* Moore and Chapman, 1986 *for cover-scale*). Five species met the criteria of dominant species in Barataria Bay, including *D. spicata*, *J. roemerianus*, *P. australis*, *S. alterniflora* and *S. patens*, of which four are grasses (*D. spicata*, *S. alterniflora*, *P. australis* and *S. patens*), and one is a grass-like rush (*J. roemerianus*).

Polyhaline marsh zones (salinity 8–29 ppt) of Barataria Bay are dominated by *S. alterniflora* and *J. roemerianus* with *J. roemerianus* more frequently dominant in the mesohaline zones (salinity 4–18 ppt: Chabreck, 1972; Visser et al., 1998). Additionally, *P. australis* is commonly present in patches as a dominant in mesohaline zones. Commonly intermixed with these dominants are the subdominants, *D. spicata*, *S. patens*, *Schoenoplectus americanus* and *Schoenoplectus robustus*. *D. spicata* and *S. patens* are found as dominants in mesohaline zones, and *D. spicata* is commonly present in polyhaline, irregularly flooded zones as a dominant, and particularly in locations where a disturbance has recently occurred (Chabreck, 1972; Visser et al., 1998).

All five species differ in the timing of peak productivity and in the volume of dead biomass buildup, which impacts their spectral profile, or reflectance. The two extreme species, in terms of fluctuations in biomass and seasonality, are *S. alterniflora* and *S. patens*. *S. alterniflora* has the most seasonal fluctuations of biomass, and consistently exhibits peak biomass in September, while *S. patens* grows throughout the year and the biomass shows little, if any, seasonal pattern (Kirby and Gosselink, 1976; Morris and Haskin, 1990; Pezeshki and DeLaune, 1991).

2.2. Image acquisition and preprocessing

In an effort to investigate the large-scale impacts and monitor the long-term recovery of coastal ecosystems following the DWH oil spill,

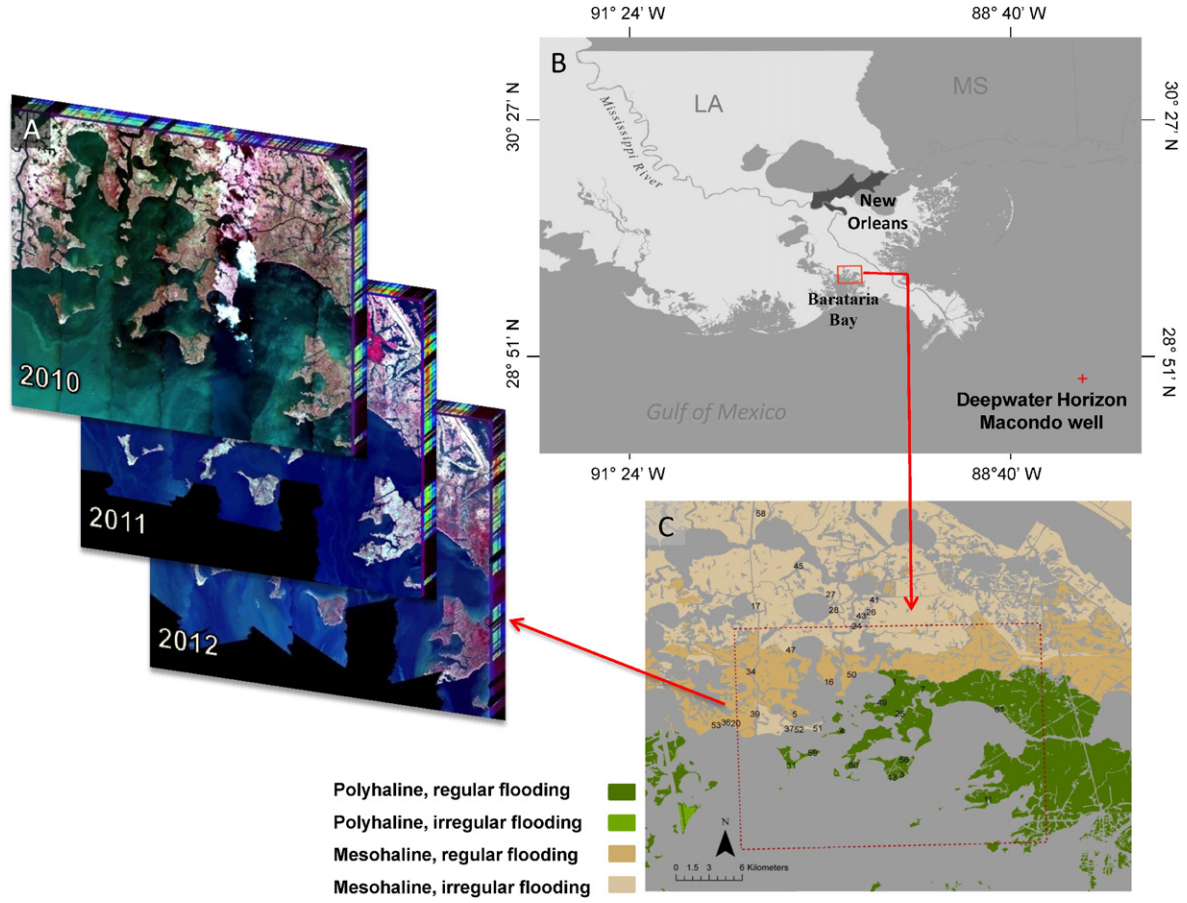

Fig. 2. Maps show the A) three AVIRIS image mosaics used for classification, B) location of study area (red box) and Deepwater Horizon well (red cross) in Louisiana, and C) field collection sites (n = 59) for reference polygons in Barataria Bay. The spatial distribution of salinity and flooding conditions is based on U.S. Fish and Wildlife Service's National Wetlands Inventory maps.

the National Aeronautics and Space Administration (NASA) deployed the ER-2 and Twin Otter International aircrafts equipped with AVIRIS to collect spectrometer data of the post-spill environment. AVIRIS is a whiskbroom scanner that measures upwelling radiance between 365 and 2495 nm at 10 nm intervals (total of 224 bands) (Green et al., 1998), and produces 700–800 ortho corrected pixels for 224 detectors on each scan. Here, the AVIRIS data used for analysis and mapping were collected for ecosystem impact assessments while deployed on the Twin Otter in October 2010, 2011 and 2012 and had a native resolution of 3.3–3.5 m (http://aviris.jpl.nasa.gov/) (Fig. 2A). The images were acquired with full navigation and georectification information.

The AVIRIS radiometric calibration took place at the Jet Propulsion Laboratory (JPL). Following image acquisition, atmospheric calibration and reflectance retrieval was performed in two steps using ACORN 6 (ImSpec LLC, Seattle). ACORN 6 performs forward inversion that fits modeled radiance against measured radiance to retrieve surface reflectance based on geographic, temporal and atmospheric parameters. In this study, water vapor was fit using the 940 nm water vapor band. After initial reflectance retrieval, a ground target was used to remove high frequency noise in retrieved reflectance (Clark et al., 2002).

Georectification was completed in two steps, starting with a geocorrection procedure using JPL's georeferencing information derived from inertial navigation data and GPS in a geographic lookup table (Boardman, 1999). Further georeferencing was done using Aerometric Inc. (http://gis.aerometric.net/dirlists.htm) aerial photos (0.30 m^2) as base maps that were resampled by pixel aggregation to 3.5 m to more closely match the resolution of the first AVIRIS datasets. Registration error of less than one pixel (RMSE < 1.0) was achieved for all images.

Environmental conditions are confounding factors in multitemporal analysis of vegetation cover, and therefore, studies commonly seek to acquire data under similar illumination, hydrologic and phenological conditions (Rogan et al., 2002). AVIRIS collection is generally restricted to within two hours of solar noon, due to the increased atmospheric scattering (atmospheric noise) that occurs early and later in the daytime hours. Atmospheric conditions were favorable (i.e. low humidity and cloud-free) on all three dates. A gap in coverage exists for the October 4, 2010 data. We attempted to fill this gap with a dataset from an earlier date (September 24, 2010), but poor atmospheric conditions made calibration unsatisfactory. Therefore, we excluded this area from the analysis for all three dates.

The AVIRIS collection dates had a maximum separation of 16 days on the Julian calendar (julian dates 277, 288, 293). However, the precipitation patterns preceding the October collection dates varied appreciably from year-to-year, likely causing variable phenological conditions (Fig. 3C). As a result, spectral signatures also varied for some species (Fig. 3A & B). The 2010 water year (October 2009–September 2010) was the wettest and vegetation was generally greener on 2010 imagery. Precipitation in both 2011 and 2012 was below average in relation to the 44-year climate record (Galliano, LA), which may have contributed to the differences in spectra (Fig. 3B & C). For instance, all species but *J. roemerianus* showed increased reflectance in the red region and red-edge shifts in the later October dates, which implies a shift from green to yellow and brown vegetation caused by the onset of natural senescence (Fig. 3B).

Tidal conditions at the time of AVIRIS data acquisition are important because varying water levels can affect image registration (i.e. shorelines differ on multitemporal datasets) and classification results (Jensen et al., 1993, Allen et al., 2012). AVIRIS data capture in northern Barataria Bay occurred between 16:39 and 19:27 UTC on October 4, 2010. Tide levels over that timeframe ranged from 0.246 to 0.138 m

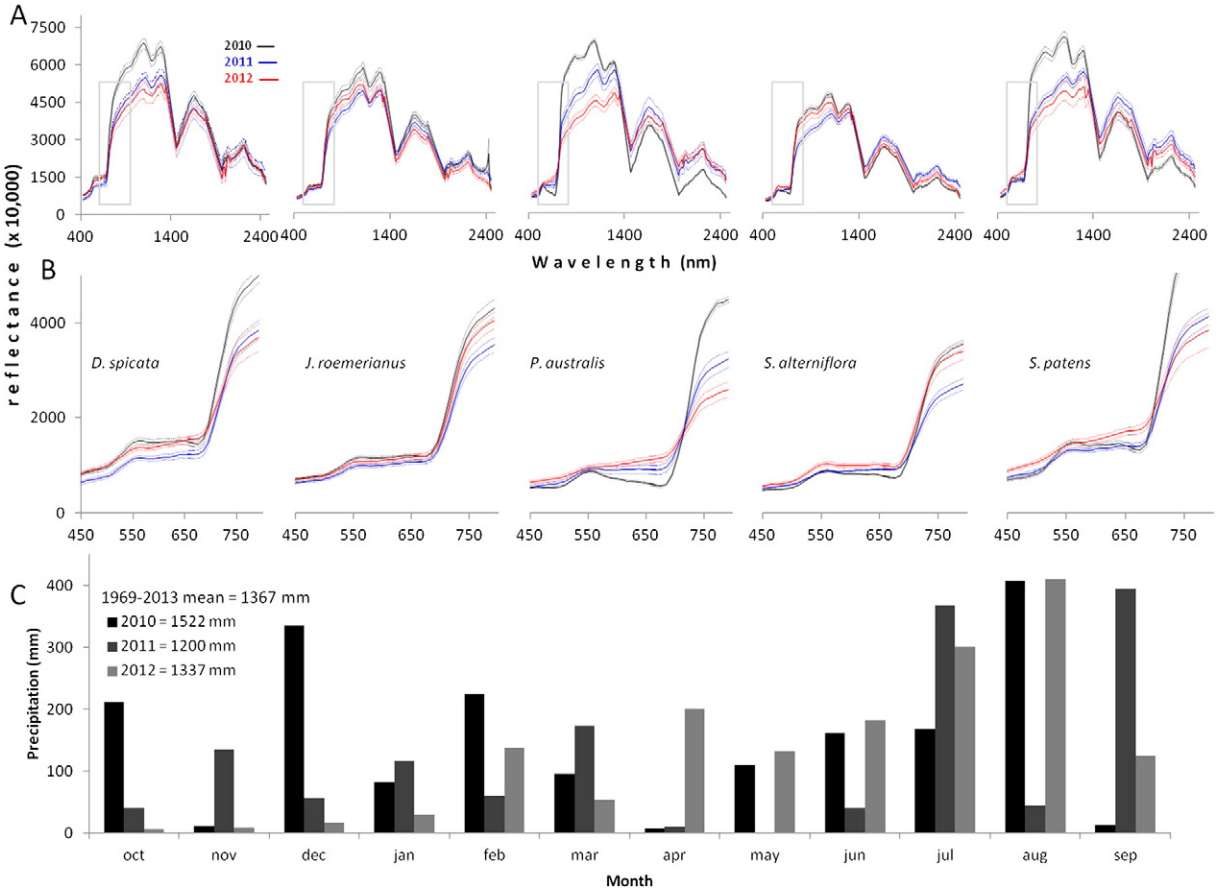

Fig. 3. Shows the full spectrum (A) and subset (B) mean reflectance curves (solid line) with 95% confidence intervals (dashed lines) of dominant species training data and monthly precipitation (C) for each water year leading up to the AVIRIS collection dates.

above mean lower low water height (MLLW: NOAA Station ID 8761724, Grand Isle, LA). On October 15, 2011, data capture occurred from 16:22 to 18:04 PM UTC with tides ranging from 0.026 to 0.036 m above MLLW. On October 19, 2012, data capture occurred from 15:48 to 17:11 PM UTC with tides ranging from 0.097 to 0.034 m above MLLW. The AVIRIS collection time on the two later acquisition dates (October 15, 2011 and October 19, 2012) were during lower tides, and therefore any decreases in land cover on those dates would not be due to higher water levels. Water levels were highest on the first image date, so the use of that image as the base layer for identification of increased open water would result in conservative estimates of the area experiencing conversion to open water.

2.3. Data collection, spectral library development & endmember selection

Classification accuracies are highly dependent upon: a) how representative the collected reference spectra are of the classes of interest (Foody et al., 1995; Chen and Stow, 2002), and b) whether the spectral separability among classes is greater than the variability within a class (Somers et al., 2011). Spectra used for classification can be collected from measurements of reflectance taken from the field, lab or imagery. Here, we used image-derived spectra because image pixels can more effectively capture the broad range in live (green) and senesced vegetation composition as well as the background components (i.e. water or soil) found in scenes (Fig. 4). Selecting pixels that cover a single class is difficult, due to the composite nature of surface materials, resulting in problems with class separability (Somers et al., 2009). We used field-referenced polygons of relatively pure stands to minimize class intermixing that may result in classification error.

Class training spectra (herein referred to as endmembers) were collected from spatially referenced dominant species polygons overlaid onto AVIRIS image mosaics for each date. To minimize spectral mixing of dominants and subdominants or understory species, selected training data were limited to dense monotypic stands by using only the Braun-Blanquet cover-abundance category 6 range (75–100% cover). Image-derived endmembers were collected from reference polygons of dominant species stands delineated during field visits in October 2012 and May and October of 2013. Field polygons ($n = 95$) of variable size were delineated using a global positioning system (GPS) and species percent cover estimates were recorded (Fig. 2C). Due to a lack of large stands observed during field visits, supplemental polygons were established for *P. australis* using the 2007 CRMS coast-wide vegetation survey (Sasser et al., 2008; *see* Visser et al., 1998 *for details in regards to Louisiana coast-wide vegetation survey methods*). Endmembers for water and soil classes were collected using visual spectra interpretation, and oil endmembers were selected using a hydrocarbon absorption index to detect oil on marsh surfaces (Kühn et al. 2004). In total, 9639 image spectra from 281 field-delineated polygons were used for training and validation of dominant species and non-vegetated surfaces, including wet and dry soil, water/glint and oiled-marsh.

The full spectral library of classes was separated into training and validation datasets. Polygons from each image date, comprising at least two-thirds of the spectra for a given class, were reserved for validation of classification results. Next, image spectra were selected from training and validation polygons, until one of two predefined thresholds was met to ensure that both small and large polygons were well-represented in the training and classification testing process, either an absolute sampling limit of 50% of the spectra from a polygon, or a limit of 10 spectra (Roth et al., 2012). The percentages of image spectra used in classification training for all classes ranged 4–15%, and for validation ranged 15–27%. The percentages were determined by the number of polygons, number of image spectra per polygon and the aforementioned thresholds for partitioning. A total of 547 image endmembers were used for classification training. A summary of the reference polygons, total image spectra and endmembers (i.e. training pixels) for each class is shown in Table 1. Twenty random training and

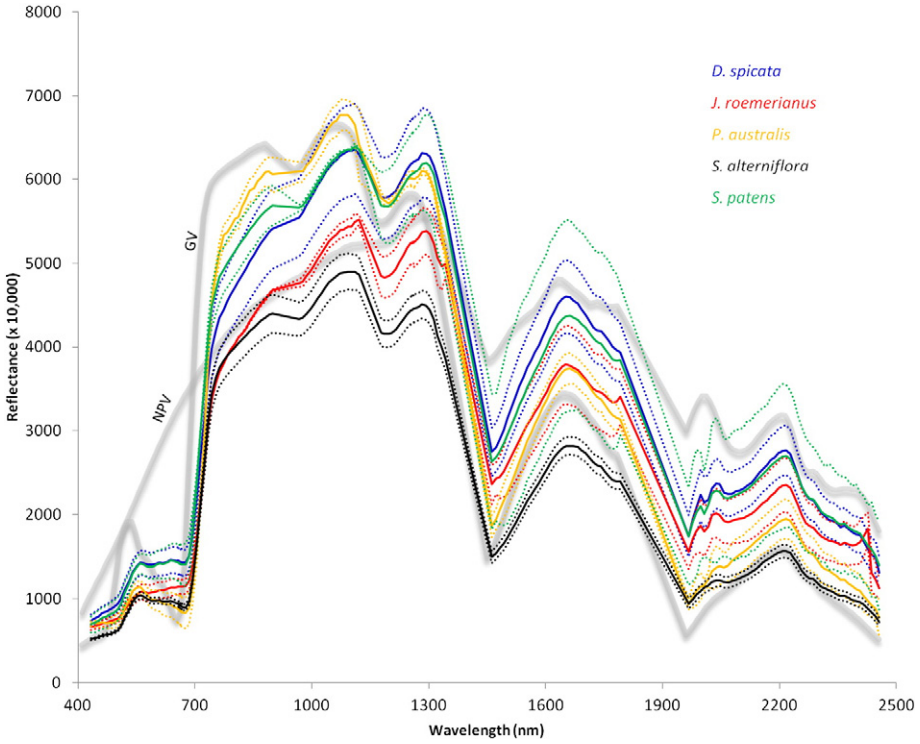

Fig. 4. Mean spectral profiles and 95% confidence intervals for the five dominant species (*Distichlis spicata*, *Juncus roemerianus*, *Phragmites australis*, *Spartina alterniflora*, *Spartina patens*), and examples of "pure" green vegetation (GV: *S. alterniflora*) and non-photosynthetic vegetation (NPV: *S. alterniflora*). Training data (image spectra) of dominant species are composites of mostly live vegetation, but also include dead vegetation, water and soil. Image spectra of dominants differ from "pure" GV and NPV endmembers (gray), and illustrates where spectral confusion among species classes is likely occur.

Table 1
Summary table of Dominant Species dataset, including reference polygons, total reference spectra (pixels), training and test samples.

Class name	Polygons	Total pixels	Training	Validation
Distichlis spicata	19	597	41	87
Juncus roemerianus	29	742	41	144
Phragmites australis	51	1898	91	228
Spartina alterniflora	78	3127	135	346
Spartina patens	21	570	38	97
Soil	3	100	15	24
Water	72	2362	185	290
Oiled marsh	2	7	1	2

validation libraries were generated and tested for CDA classification. Generating the relatively large number of paired training and validation libraries was considered an important step, due to the potential intrinsic variability of the image spectra.

2.4. CDA classification

CDA was applied to the training data to maximize the between-class variance by selecting bands with significant discriminating power, and discarding unexplained noise and redundancy (Pu and Liu, 2011; Alonzo et al., 2013). A set of standardized coefficients were multiplied through the original spectra in MATLAB (The Mathworks, Inc., 2012) to derive canonical weighted functions (one per band), and determine the bands which are significant contributors to class discrimination (Roth et al., 2015). Following CDA dimension reduction, a linear discriminant classifier was used in ENVI/IDL (www.exelisvis.com) to assign image spectra to the class that produces the highest discriminant function score. AVIRIS image mosaics were classified (October 2010, 2011 & 2012), and a post-classification majority vote of the 20 different maps generated by the random training pulls was used to eliminate noise in areas of higher classification inconsistency, and improve overall map outputs.

2.5. Map validation

Two data sets were used to validate the dominant species classification maps. The first assessment was done using spectra in the validation dataset that were excluded from the random sampling process. A total of 7043 pixels were used as validation spectra for each of the 20 random pairs of training and validation libraries, and confusion matrices were assessed for errors of omission (producer error) and commission (user error) among classes (species).

A classification performance assessment was conducted using U.S. Geological Survey (USGS) post-oil spill vegetation surveys (USGS unpublished data). Researchers from the USGS revisited six sites (three oiled and three non-oiled) contemporaneously with AVIRIS collection in October 2010, 2011 and 2012 (Fig. 5A & B). The surveys consisted of four 4 m^2 plots along three 50 m transects that were spaced 30 m apart for a total of 72 plots. The 12 plots from site 5 were excluded from the classification assessment because it was located in the data gap in the October 2010 image. Transects A, B and C were positioned from west to east at each site, and plots were randomly spaced along each 50 m transect with plot 1 being the closest and plot 4 being the farthest from the shoreline. This dataset provided field observations of species composition that corresponded with AVIRIS collection dates. Observations included species identification and richness, cover fractions and abundance estimates of live, green (GV) and senesced, non-photosynthetic (NPV) vegetation. Using this dataset for classification validation introduces several challenges and limitations. For instance, the reliability of classification evaluation is potentially diminished, due to georectification error of up to one pixel (12.25 m^2) and the uncertainty of the GPS accuracy for the plot locations (~5 m). Because of differences in plot and pixel size, and positional uncertainty, we created 2 m buffers around the USGS plots. We evaluated the classification performance based on one or more pixels within the 4 m^2 buffer area being classified as the targeted species.

Some of the dominant species are not represented well by the reference dataset, as 95% of the observations were either *S. alterniflora* or *J. roemerianus*. Therefore, the validation library (first approach) is the more comprehensive method, but the USGS plots provide an assessment of each individual map in the time series, and validation by shoreline zone. We defined the dominant species as the one with the highest cover fraction per plot, because some plots lacked a dominant with GV cover >50%.

2.6. Oiled and non-oiled shoreline identification

Marsh oiling was concentrated in the first 15 m of the shoreline with a maximum distance of 21 m (Silliman et al., 2012; Khanna et al., 2013; Kokaly et al., 2013; Peterson et al., 2015). Therefore, the focus of our analysis of dominant species distributions was on the shoreline zones. To establish a shoreline vector, we masked all pixels that were modeled

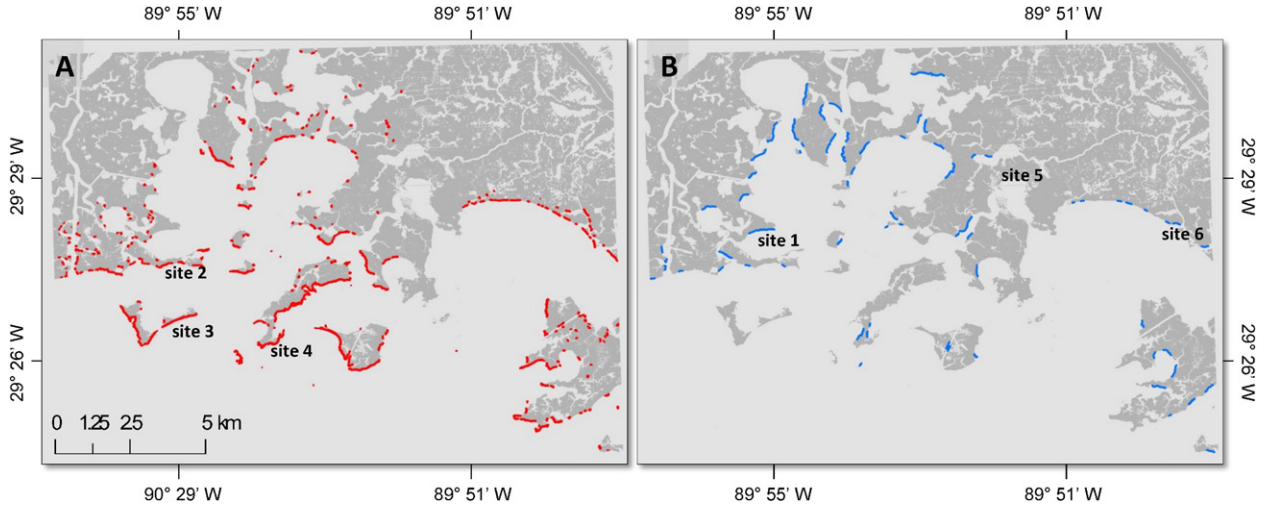

Fig. 5. USGS site locations are shown on study area maps of A) oiled, B) and non-oiled shoreline zones (red) in similar landscape positions.

as GV, NPV, oiled vegetation or soil that summed to ≥5%. We used 5% to match minimum fraction criteria used in model selection by Multiple Endmember Spectral Mixture Analysis (MESMA: Roberts et al., 1998; Halligan, 2002; Dennison and Roberts, 2003). Next, we removed mudflats and lakes located within the marsh interior that had no connectivity with large channels and bays by converting the raster of water pixels into a polygon. We separated the multi-part polygons into individual features, and deleted the features that were disconnected from the Barataria Bay polygon. This procedure removed shorelines that we assumed would not have been exposed to oil following the DWH spill (Khanna et al., 2013). An 8 pixel (28 m) buffer from the edge pixels was used to create shoreline zones.

Oiled marsh cover was determined using MESMA (Roberts et al., 1998; Peterson et al., 2015), because oil fractions (per pixel) generated with MESMA provide a more comprehensive spatial coverage of oil than produced by discrete CDA classification. For a detailed description of the method used to generate oil fractional cover, refer to Peterson et al. (2015). In summary, iterative endmember selection (IES: Roth et al., 2012) was used to produce a spectral library of GV, NPV, soil and oiled marsh endmembers. Stable Zone Unmixing (SZU: Somers et al., 2010), InStability Index (ISI: Somers et al., 2009) and synthetic mixture modeling were used to identify an optimal subset of bands for discriminating endmembers. Finally, two, three and four endmember models were run on each image, followed by an automated extraction process in which endmember combinations with the lowest RMSE and least complexity (fewest endmembers) were selected for each pixel and merged into a multiple endmember fractional cover dataset.

We created a mask of pixels that were oiled (≥5% oil fraction) using AVIRIS images (same spatial resolution) from September 14, October 4, 2010 and May 4, 2011 to capture maximum oil coverage, and applied it to the mask of the shoreline zone maps (Fig. 5A). The mask was used to examine the changes in marsh vegetation cover at oiled locations and to compare change in oiled marshes to changes in marshes that were not affected directly by oil, but were in a similar landscape position (elevation and distance from shoreline). Furthermore, we refined the non-oiled zone filter to only include shorelines that were oriented towards the south (90° to 270°) as these were the locations most heavily contaminated by oil (Khanna et al., 2013; Kokaly et al., 2013; Peterson et al., 2015) (Fig. 5B).

3. Results

3.1. Spectral library (endmember) and classification validation

Twenty randomly sampled (paired) training and validation libraries were spectrally transformed into CDA functions and assessed for classification performance using a linear classifier in MATLAB 7.9. Twenty paired libraries had an average overall accuracy of 82% and kappa of 0.78 (Table 2). Little variability was found among classification accuracies for all training libraries, so we opted to use all libraries for CDA classification and a majority rule classifier to aggregate the final results. Average producer's and user accuracies for the species classes was 72% (Table 2). The highest accuracies (producer) were for *S. alterniflora* and *J. roemerianus*, and *P. australis* and *S. alterniflora* reported the highest classification reliability (user) (Table 2). As expected, accuracies were higher for non-vegetated classes with the exception of oiled marsh, which had a small sample size (Table 2). We anticipated *D. spicata* and *S. patens* would be difficult to distinguish, due to their similar morphology and spatial association. *S. patens* reported the lowest combined accuracy and reliability, while *D. spicata* reported the lowest reliability overall. Yet, *D. spicata* endmembers were more likely to be confused with *J. roemerianus* and *S. alterniflora* (Table 2). Confusion occurred among the *Spartina* species (*S. patens* misclassified 30% of training samples as *S. alterniflora*). However, as expected, the spatial distribution of *S. patens* dominance is most commonly classified in the northern portion of the study area where the marshes transition from polyhaline (indicator species *S. alterniflora*) to mesohaline (indicator species *S. patens*) (Fig. 6: Visser et al., 1998).

3.2. Dominant species distribution

A total of 41,248,359 m^2 were classified as one of the five dominant species, soil, water (shallow water, deep water and glint), or oiled marsh (Fig. 6; Table 3A). *S. alterniflora* was the most widespread over all three years, averaging 76% cover, followed by *J. roemerianus* (9%), *S. patens* (9%), *D. spicata* (3%) and *P. australis* (1%) (Fig. 6; Table 3A). The percent cover was relatively stable between years for the less common dominants, however, *S. alterniflora* and *J. roemerianus* exhibited considerable change (Table 3A). There was an overall loss of 7% (2,909,585 m^2) of the marsh area to open water from 2010 to 2012, with a greater loss occurring from 2011 to 2012 (1,807,285 m^2) (Table 3A).

S. alterniflora and *J. roemerianus* covered >80% of the marsh area in the oiled and non-oiled shoreline zones (Fig. 5; Table 3B & C). Distributions of species in oiled and non-oiled shoreline zones changed substantially during the two periods, however, the distribution patterns were similar for both zones. *S. alterniflora* decreased markedly from 2010 to 2011 and remained relatively stable from 2011 to 2012 in both oiled and non-oiled shoreline zones (Table 3B & C). *J. roemerianus* increased substantially from 2010 to 2011 and decreased slightly from 2011 to 2012 in both oiled and non-oiled shoreline zones (3B & C). *D. spicata* exhibited similar increases from 2010 to 2011 and decreases in 2011–2012 in oiled and non-oiled shoreline zones (Table 3B & C). *S. patens* increased in oil zones and decreased in non-oiled shoreline zones from 2010 to 2011, and decreased in both oiled and non-oiled zones from 2011 to 2012. *P. australis* cover was negligible in 2010 and 2011, but increased considerably from 2011 to 2012 in both oiled and non-oiled shoreline zones (Table 3B &C).

Table 2
Matrix of training endmember allocations, producer and user accuracies and averaged kappa and overall accuracies for the 20 sample libraries.

	D. spicata	*J. roemerianus*	*P. australis*	*S. alterniflora*	*S. patens*	Soil	Oiled marsh	Water	Unclassified
D. spicata	**61**	17	14	14	6	0	0	0	0
J. roemerianus	17	**108**	7	22	4	0	0	0	0
P. australis	2	0	**157**	6	0	0	0	0	0
S. alterniflora	5	16	23	**300**	29	0	0	0	0
S. patens	1	3	27	3	**58**	0	0	0	0
Soil	0	0	0	0	0	**24**	0	0	0
Oiled marsh	1	0	0	0	0	0	**2**	0	0
Water	0	0	0	1	0	0	0	**290**	0
Unclassified	0	0	0	0	0	0	0	0	0
Producer (%)	70	75	69	87	60	100	100	100	
User (%)	54	68	95	80	63	100	67	100	
Overall accuracy (%)	82.10								
Kappa	0.78								

Bold characters indicate the number of correct allocations.

Fig. 6. Highlighted marsh dominants (red) for 2010 (top), 2011 (middle) & 2012 (bottom). *Spartina alterniflora* covered 70% of the marsh area, followed by *Juncus roemerianus* with 14% and *Spartina patens* with 10%.

Table 3
Coverage area and percent cover per dominant species and non-vegetation classes for 2010, 2011 & 2012 in full study area, oiled shoreline zones and non-oiled shoreline zones. DISP = *Distichlis spicata*; JURO = *Juncus roemerianus*; PHAU = *Phragmites australis*; SPAL = *Spartina alterniflora*; and SPPA = *Spartina patens*.

Full study site	2010 (m^2)	% Cover	2011 (m^2)	% cover	2012 (m^2)	% cover
DISP	554,082	1	2,126,780	5	957,628	2
JURO	1,496,604	4	5,530,035	14	3,861,497	9
PHAU	95,093	0	53,863	0	766,352	2
SPAL	35,514,804	87	27,721,139	68	29,491,320	72
SPPA	3,236,254	8	4,421,259	11	2,966,840	7
Dry soil	1934	0	539	0	2338	0
Oiled	59,470	0	2326	0	2681	0
Water	0	0	1,102,300	3	2909,585	7
Total	40,958,241		40,958,241		40,958,241	
Oiled zone						
DISP	76,498	3	216,922	10	146,031	7
JURO	228,944	10	333,316	15	261,066	12
PHAU	25,242	1	7798	0	63,314	3
SPAL	1,801,580	80	1,444,124	64	1,446,976	65
SPPA	51,562	2	130,900	6	47,779	2
Dry soil	575	0	135	0	539	0
Oiled	57,058	3	220	0	453	0
Water	0	0	108,045	5	275,303	12
Total	2,241,460		2,241,460		2,241,460	
Non-oiled zone						
DISP	27,336	4	64,746	10	42,417	6
JURO	83,953	12	157,709	23	143,827	21
PHAU	6757	1	1126	0	25,426	4
SPAL	521,788	77	392,541	58	403,118	60
SPPA	33,505	5	27,213	4	15,461	2
Dry soil	0	0	0	0	0	0
Oiled	49	0	0	0	12	0
Water	0	0	30,053	4	43,127	6
Total	673,389		673,389		673,389	

Cover change detection from 2010 to 2012, in areas initially dominated by *S. alterniflora* and *J. roemerianus*, indicate that marsh area loss was proportionately similar for both species in oiled shoreline zones. Marsh loss to open water for both species was higher along oiled shorelines (12% and 10%, respectively) than non-oiled shorelines (7% and 4%, respectively). *S. alterniflora* retained a comparable proportion of its initial cover distribution in oiled (72%) and non-oiled (69%) shoreline zones, however, *J. roemerianus* retained 20% less of its initial cover distribution along oiled shorelines (37% and 57%, respectively). *J. roemerianus* was largely converted to *S. alterniflora* (34%) along oiled shorelines, while only 8% of *S. alterniflora* converted to *J. roemerianus*. A relatively small percentage changed to any of the three other classified dominants (<5% for *D. spicata*, *P. australis*, *S. patens*) in oiled and non-oiled zones.

The overall loss of vegetated marsh in the oiled zone was 12% compared to 6% in the non-oiled zone, as indicated by the increases in water classes found in oiled (0% to 5% to 12%) and non-oiled (0% to 4% to 6%) zones (Table 3B & C). The loss of *S. alterniflora* from 2011 to 2012 is not replaced by the other marsh dominants. Rather, it largely transitions to the water class indicating a net loss of marsh area.

3.3. Site-specific assessments of dominant species maps

The data used for map validation (USGS) were not collected for the purposes of assessing discrete classification performance. Rather, the surveys were conducted to evaluate plot-scale changes in community composition, and to measure belowground and aboveground biomass. Consequently, the quantity (i.e. 60 plots) and spatial distribution of sites is limited, in part due to the time-consuming nature of the data being collected. The USGS sites were the only data available that could be used to evaluate multitemporal classification performance, and to document the change in cover at both oiled and non-oiled shoreline

locations. USGS data were used to examine species composition and plot-specific cover attributes in comparison with classification maps to assess the performance of the classifier on a per-pixel basis.

Overall, CDA classifications were consistent with field observations across sites with 84% agreement between USGS plots and CDA classified maps, and the lowest accuracy reported for site 1 (75%) and the highest accuracy for sites 2 & 3 (94%). The dominant species were mapped accurately for 82% of the USGS plots in 2010, 82% in 2011 and 88% in 2012. The overall accuracy based on the USGS field observations (84%) was comparable to the spectral library validation accuracy (82%). When the USGS observations were separated into Braun-Blanquet cover-abundance category 6 (>75%) levels and below, the classifier was 88% accurate for ≥75% single dominant cover and 82% accurate for <75% cover of a single dominant, indicating spectral mixing of dominants is accountable for some class confusion. In general, CDA-classifications were more accurate for plots >25 m from both oiled and non-oiled shorelines. For plots farther than 25 m from the shoreline, the classified maps were in 89% agreement with field observations, while plots within 25 m of the shoreline were 80% accurate.

From 2010 to 2012, all plots at non-oiled sites (sites 1 & 6) had >80% vegetation cover and an overall decrease in cover of 4% and 7% (Fig. 7). Of the plots closest to the shoreline, only C1 exhibited a decrease in vegetation cover of >10% (95% to 80%), suggesting that shoreline erosion did not occur or was minimal at these non-oiled sites (Fig. 7; Table 4).

USGS field sites 2, 3, & 4 were impacted by heavy oiling in 2010 and exhibited signs of oil-induced vegetation stress, including widespread chlorosis and plant mortality, particularly in the plots that were closest to the shoreline. Field observations indicated site 4 was the most heavily oiled site with oil covering both the vegetation stems and/or soil substrate. Oil was present on plant stems and soil substrate in five of the six plots that were closest to the shoreline at site 4, and vegetation in these plots exhibited near-complete mortality (>90%: Table 5). Plot C2 was the only plot within 15 m of the shoreline to show signs of live vegetation cover (98% live) with only light oil impact to vegetation stems (Table 5). The CDA map successfully classified oil in the five plot locations with oil cover, and correctly classified plot C2 as *S. alterniflora*. Site 3 was also extensively oiled with plots A1, B1 and C1 showing heavy impacts, including 70% (C1) and 40% (A1 & B1) plant mortality (Table 5). CDA successfully classified A1 as oiled marsh (Fig. 8; Table 5). Plot B1 was inhabited by *J. roemerianus* (40%) and *S. alterniflora* (30%), and CDA classified the two pixels encompassed by the plot as *J. roemerianus* and *S. patens* (Fig. 8; Table 5). Plot C1 was inhabited by *S. alterniflora* (20%) and *D. spicata* (10%), and this location was misclassified as *J. roemerianus* (Fig. 8; Table 5). At plots A1 and C1 of site 2 near-complete mortality (>90%) was also observed, and the CDA map successfully identified the oiled-vegetation in these plot locations (Fig. 8; Table 5).

All plots that showed heavy oiling exhibited plant stress (>50% chlorosis) in 2010, however, mortality was not observed at all plots. For example, heavy oiling and >50% chlorosis was observed at plots B1 and B2 of site 2, but plant mortality was <10%, and CDA successfully classified these plots as *J. roemerianus* (Fig. 8; Table 5). Plots A3, B3 and C3 of site 4 showed only light oiling and live vegetation cover between 85 and 90%, and these plots were classified accurately as *J. roemerianus* (A3) and *S. alterniflora* (B3 & C3: Fig. 8; Table 5). Plots A4, B4 and C4 all had live vegetation cover >70%, and exhibited only trace oil impacts (i.e. speckled chlorosis on stems) with no visible oil present on stems or substrate. CDA misclassified one of these plots as *S. alterniflora* (A4), and classified accurately plots B4 and C4 as *S. alterniflora*. *S. alterniflora* dominated cover with only trace oil impacts were observed at the nine plots >5 m from the shoreline at site 3, and the 2010 CDA map was correctly classified as *S. alterniflora* for all these plot locations (Fig. 8; Table 5).

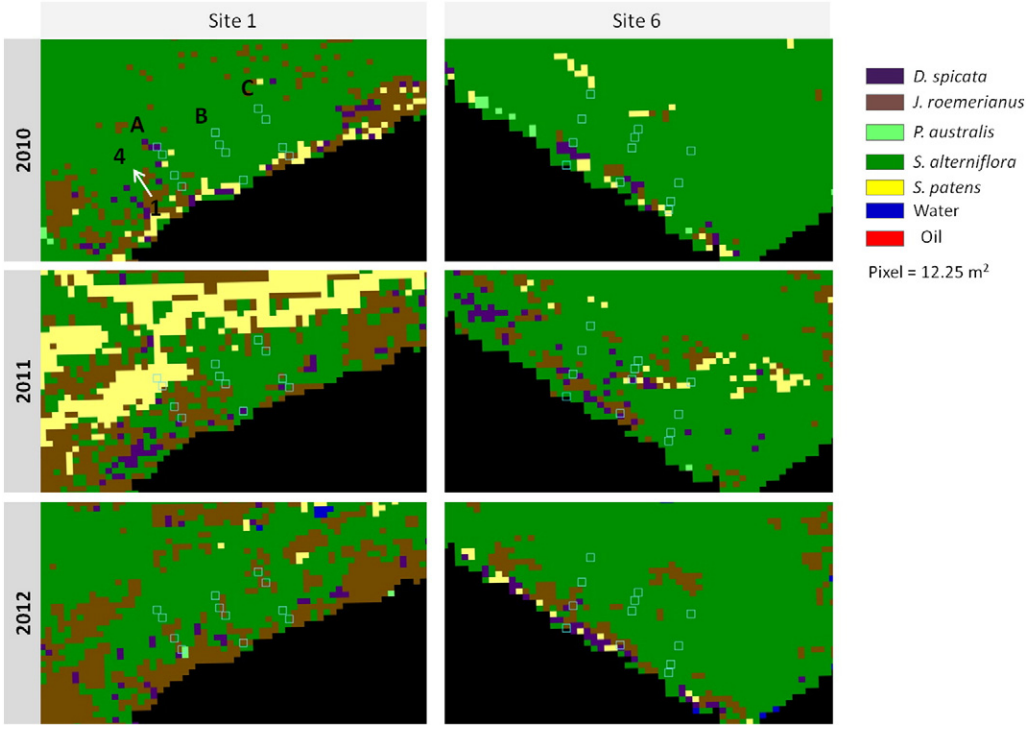

Fig. 7. Location of plots (light blue square, N = 24) used for 2010, 2011 & 2012 classification and survey comparisons of USGS non-oiled sites 1 & 6. Four randomly positioned plots (1 closest and 4 farthest from shoreline) were located along transects A (west), B (middle) and C (east). Black pixels represent initial (2010) open water.

Table 4
Prevalent species and cover-abundance at non-oiled site 1 (left) and site 6 (right) in 2010, 2011 and 2012 from USGS plots (1–4).

2010	Transect A	Transect B	Transect C	2010	Transect A	Transect B	Transect C
1	JURO(98)	JURO(69)	JURO(40)	1	SPAL(10)	DISP(10)	SPPA(15)
			SPAL(45)		DISP(30)	SPAL(30)	DISP(40)
2	JURO(95)	SPAL(15)	SPAL(80)		SPPA(45)	JURO(75)	SPAL(85)
		JURO(45)		2	SPAL(10)	SPAL(30)	SPAL(98)
3	SPAL(10)	SPAL(30)	SPAL(40)		JURO(60)	JURO(65)	
	JURO(85)	JURO(60)	JURO(50)	3	SPAL(85)	SPAL(85)	SPAL(98)
4	SPAL(10)	JURO(30)	SPAL(25)	4	SPAL(75)	SPAL(90)	SPAL(90)
	JURO(88)	SPAL(50)	JURO(70)				
2011				2011			
1	JURO(45)	JURO(20)	JURO(40)	1	DISP(13)	JURO(15)	SPPA(20)
	SPAL(54)	SPAL(80)	SPAL(60)		SPPA(80)	SPAL(15)	SPAL(70)
2	JURO(45)	SPAL(15)	SPAL(95)			SPPA(40)	
	SPAL(54)	JURO(80)		2	SPAL(10)	JURO(15)	SPAL(90)
3	SPAL(49)	SPAL(35)	JURO(80)		JURO(85)		
	JURO(60)	JURO(45)		3	SPAL(70)	SPAL(40)	SPAL(70)
4	JURO(6)	JURO(15)	JURO(<5)	4	SPAL(50)	SPAL(60)	SPAL(30)
	SPAL(<5)	SPAL(80)	SPAL(<5)				
2012				2012			
1	SPAL(40)	JURO(10)	JURO(15)	1	DISP(10)	SPPA(10)	SPPA(10)
	JURO(45)	SPAL(85)	SPAL(75)		SPAL(10)	SPAL(15)	SPAL(50)
2	JURO(40)	SPAL(10)	JURO(10)		SPPA(40)	JURO(65)	
	SPAL(50)	JURO(75)	SPAL(80)	2	JURO(50)	SPAL(30)	SPAL(93)
3	SPAL(50)	SPAL(10)	SPAL(15)		SPAL(<5)	JURO(45)	
		JURO(35)	JURO(55)	3	SPAL(77)	SPAL(75)	SPAL(95)
4	SPAL(70)	SPAL(25)	JURO(20)			JURO(<5)	JURO(<5)
		JURO(50)	SPAL(35)	4	SPAL(70)	SPAL(80)	SPAL(70)
						JURO(<5)	

Additionally, *D. spicata* was classified in pixels adjacent to the plots and observed as a subdominant in plots in 2011 and 2012 (Fig. 8; Table 5).

Heavy oiling of stems and soil substrate was only seen at site 4 in 2011. Heavy oiling and dead stems were observed at A1 & C1 of site 4. These plots were characterized by low to no live aboveground biomass (<15%), while B1 showed heavy oiling, but *S. alterniflora* live biomass of 75% (Fig. 8). The 2011 CDA map did not classify plots A1 & C1 as oiled, but captured the *S. alterniflora* in plot B1. All other plots of site 4 were classified accurately as *S. alterniflora* with the exception of C4, which was reportedly a mixed plot of *J. roemerianus* and *S. alterniflora*, but with low live vegetation cover (40%) (Fig. 8).

The CDA classifier had some difficulty with plots at sites 2 and 3 where vegetation had begun to recover in 2011, due to the lack of a single, clear dominant in the plots and apparent increase in species richness (Table 5). For instance, no oil was observed on stems or substrate within plots A1, B1 or C1 of site 3, and only trace impacts were observed to stems (speckled chlorosis). Vegetation had largely recovered and was characterized by mixtures of *S. alterniflora*, *D. spicata*, *J. roemerianus* and *S. patens* with live vegetation composing at least 80% of the plots (Table 5). *S. alterniflora* was observed in the field and classified for all three plots. However, *D. spicata* cover (50–60%) was dominant in plots A1 and C1, and therefore the classification of *S. alterniflora* was viewed as an error (Fig. 8; Table 5). The green vegetation on most plots were *S. alterniflora*-dominated for sites 2 and 3 with the exceptions of B3 and C4 of site 2, which were inhabited by *S. alterniflora* and *J. roemerianus* in comparable cover-abundance. The classifications were accurate for all plots 2 through 4, except for B4 which was classified as *D. spicata* and *J. roemerianus* rather than *S. alterniflora* as observed in the field (Fig. 8; Table 5).

In 2012, no oil was observed at sites 2, 3 or 4. At site 4, only four plots exhibited any vegetation cover (A2 = 15%, A3 = 95%, A4 = 15%, B4 = 30%) and only one plot had live vegetation cover of >20%. The CDA maps are in general agreement with most of the survey observations (Fig. 8; Table 5). At sites 2 & 3, *S. alterniflora* was the most abundant dominant along all transects, however, the cover was below 50% for several plots in 2012. Likewise, the classification results in those plot locations reflect *S. alterniflora* dominance. Several plots that were misclassified (e.g. A3 and C2 of site 3) had low live vegetation cover, low average stem heights (52–73 cm) and the presence of wrack (Fig. 8; Table 5).

4. Discussion

4.1. Accuracy assessment

Oiling factors, such as oil-type; timing of exposure; concentration; thickness; degree of weathering and emulsification; and surface distribution, have been shown to elicit highly variable vegetation and ecosystem responses (Pezeshki et al., 2000). Subsequent to the DWH spill, ground-based and remotely sensed surveys of oil contamination in marshes have been conducted to measure these oiling factors (Kokaly et al., 2013; Michel et al., 2013; Peterson et al., 2015). The distribution of dominant species in oil-contaminated marshes is an important factor in explaining ecosystem response. We set out to generate a time series of classified maps that consistently meet or exceed previous efforts to map salt marsh dominant species. An overall accuracy 82% (kappa = 0.78) was obtained when comparing training and validation spectra (Table 2), indicating CDA performed well in discriminating classes despite the spectral similarity of the dominant species. The CDA classifier performed well in locations with little spectral mixing among dominant species classes. For instance, the classified pixels in Fig. 9A & D are in agreement with the observations from validation polygons, despite presence of subdominant species (Fig. 9A). In contrast, the classifier performed poorly in areas characterized by wrack zones in 2011 and low vegetation cover (Fig. 9B) or intermixed dominant species in 2012 (Fig. 9C).

In comparison with a time series of field (USGS) surveys along oiled and non-oiled shorelines, CDA classifications were in agreement with 84% of the plot observations (n = 180), and in 88% agreement if plots with mixed dominants (<75%) are removed. *S. alterniflora* is clearly the most commonly occurring dominant in the polyhaline marshes of Barataria Bay, but appears to be overly classified in shoreline zones in place of *J. roemerianus* on the 2010 classified map (Fig. 6). Dense mixtures of *J. roemerianus* and *S. alterniflora* are commonly observed within ~30 m of shoreline, and due to the influence of distinctive phenological properties on spectral features, the species that is classified as dominant in a given location (i.e. pixel) may change depending on the timing of the AVIRIS data collection. *J. roemerianus*, for instance, has continuous aboveground biomass production throughout the year and lacks a clear "greening up" pattern (Hopkinson et al., 1978). Conversely, *S. alterniflora* has clear seasonal trends in aboveground green biomass with increasing live leaf production through the spring and summer (Hopkinson et al., 1978; Gosselink and Pendleton, 1984). *S. alterniflora* canopies were potentially greener in 2010, due to the greater annual rainfall leading up to the collection date (Fig. 3C). This would potentially explain some of the decrease in *S. alterniflora* and increase in *J. roemerianus* from 2010 to 2011. The seasonality of *S. alterniflora* also may be responsible for the *S. alterniflora* to *S. patens* conversion from 2010 to 2011 seen in Figs. 6 and 7. This conversion to *S. patens* is likely an artifact in the classification occurring in locations where mats of dead grass (wrack) have suppressed new vegetation growth. The large wrack zones were only observed in the 2011 data, and the inclusion of a sensenced grass class could have addressed this classification problem. However, we determined a non-specific plant class, like senesced grass, would aggregate pixels from all species classes where heavily mixtures of live and senesced grass occurred. This was considered a departure from the focus of the paper, and was excluded from the classification scheme. The accuracy of the CDA-classified maps are acceptable in comparison to previous efforts to map species in intertidal environments using imaging spectroscopy. Sadro et al. (2007) used spectral angle mapper (SAM) and a mixture-tuned matched filter to classify salt marsh vegetation species on AVIRIS images and generated overall

Table 5
Prevalent species and cover-abundance at oiled sites in 2010, 2011 and 2012 from USGS plots(1–4).

2010	Transect A	Transect B	Transect C		Transect A	Transect B	Transect C		Transect A	Transect B	Transect C
1	DISP(8)	JURO(90)	no veg	1	DISP(20)	SPAL(30)	DISP(10)	1	SPAL(8)	SPAL(<5)	no veg
	SPAL(<5)				SPAL(40)	JURO(40)	SPAL(20)	2	SPAL(90)	JURO(50)	SPAL(95)
2	JURO(85)	JURO(99)	JURO(45)	2	JURO(25)	SPPA(20)	JURO(10)	3	SPAL(25)	SPAL(85)	SPAL(90)
			SPAL(50)		SPAL(60)	SPAL(82)	SPAL(80)		JURO(60)		
3	SPAL(85)	SPAL(30)	SPAL(15)	3	JURO(15)	JURO(25)	SPAL(90)	4	SPAL(10)	JURO(10)	SPAL(34)
		JURO(68)	JURO(90)		SPAL(75)	SPAL(75)			JURO(85)	SPAL(70)	JURO(36)
4	JURO(45)	SPAL(25)	SPAL(20)	4	SPAL(93)	JURO(15)	SPAL(95)				
	SPAL(80)	JURO(65)	JURO(60)			SPAL(75)					
2011				2011				2011			
1	no veg	SPAL(15)	DISP(50)	1	SPPA(15)	SPPA(15)	SPAL(20)	1	SPAL(15)	SPAL(70)	no veg
		DISP(25)			SPAL(25)	SPAL(30)	DISP(60)	2	SPAL(10)	SPAL(98)	SPAL(80)
		JURO(35)			DISP(50)	JURO(55)		3	SPAL (<5)	DISP(10)	SPAL(45)
2	JURO(35)	DISP(20)	JURO(15)	2	JURO(15)	SPPA(10)	SPAL(80)			SPAL(55)	
	SPAL(45)	JURO(20)	SPAL(70)		SPAL(45)	SPAL(45)		4	JURO(15)	JURO(15)	SPAL(15)
		SPAL(50)		3	JURO(25)	JURO(18)	SPAL(90)		SPAL(55)	SPAL(45)	JURO(25)
3	SPAL(90)	JURO(40)	JURO(50)		SPAL(40)	SPAL(20)					
		SPAL(45)		4	JURO(10)	JURO(10)	JURO(25)				
4	SPAL(20)	JURO(10)	JURO(10)		SPPA(10)	SPAL(50)	SPAL(30)				
	JURO(30)	SPAL(80)	SPAL(35)		SPAL(30)						
2012				2012				2012			
1	SPAL(70)	SPAL(20)	DISP(40)	1	SPPA(10)	JURO(15)	SPAL(70)	1	no veg	No veg	SPAL(<5)
		JURO(30)			SPAL(85)	SPAL(60)		2	JURO(5)	No veg	No veg
2	JURO(20)	DISP(10)	JURO(25)	2	JURO(20)	SPAL(45)	SPAL(20)		SPAL(5)		
	SPAL(60)	SPAL(15)	SPAL(40)		SPAL(60)			3	SPAL(60)	No veg	No veg
		JURO(35)		3	SPAL(40)	JURO(25)	SPAL(65)	4	JURO(6)	SPAL(20)	No veg
3	SPAL(80)	SPAL(35)	JURO(60)			SPAL(40)					
		JURO(45)		4	JURO(15)	JURO(20)	SPAL(90)				
4	JURO(35)	JURO(20)	JURO(10)		SPAL(70)	SPAL(55)					
	SPAL(50)	SPAL(50)	SPAL(35)								

accuracy of 59% (kappa = 0.40). Similarly, Schmidt et al. (2004) produced wetland species maps with an overall classification accuracy of 66% (kappa = 0.64) using an expert system and HyMap imagery (Integrated Spectronics Pty Ltd). Judd et al. (2007) achieved higher classification accuracies (overall accuracy 85%, kappa = 0.76) using Navy Research Laboratory Portable Hyperspectral Imager for Low Light Spectroscopy II (PHILLS II) sensor and a linear unmixing algorithm.

4.2. Assessment of vegetation cover change

The loss in overall vegetation cover (and increase in bare soil) suggests post-spill productivity was reduced, but the conversion from dead to live vegetation also suggests there were signs of recovery. For example, green vegetation increased to 45% cover or more in the oil-impacted plots of sites 2 and 3 in 2012. *D. spicata* (40%) was dominant and the classification map was in agreement with the field observations (Fig. 8; Table 5). Additionally, the colonization by *D. spicata* following disturbance makes ecological sense as it has been described as an opportunistic species (Shumway, 1995). Previous research has suggested that *D. spicata* can more effectively compete for resources under nutrient-limited conditions than other salt marsh dominants (Levine et al., 1998). Further, in Gulf Coast marshes, it has been shown to occur as a colonizing species following disturbances, such as storm surges (Clewell et al., 1999).

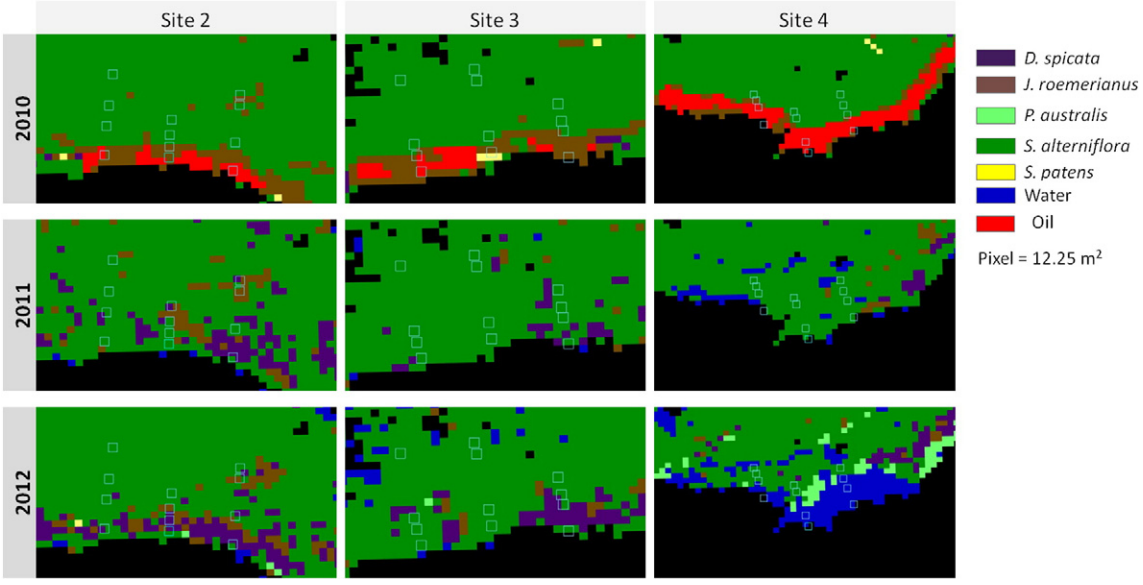

Fig. 8. Location of plots (light blue square, N = 36) used for 2010, 2011 & 2012 classification and survey comparisons with USGS oiled sites 2, 3 & 4. Four randomly positioned plots (1 closest and 4 farthest from shoreline) were located along transects A (west), B (middle) and C (east). Black pixels represent initial (2010) open water.

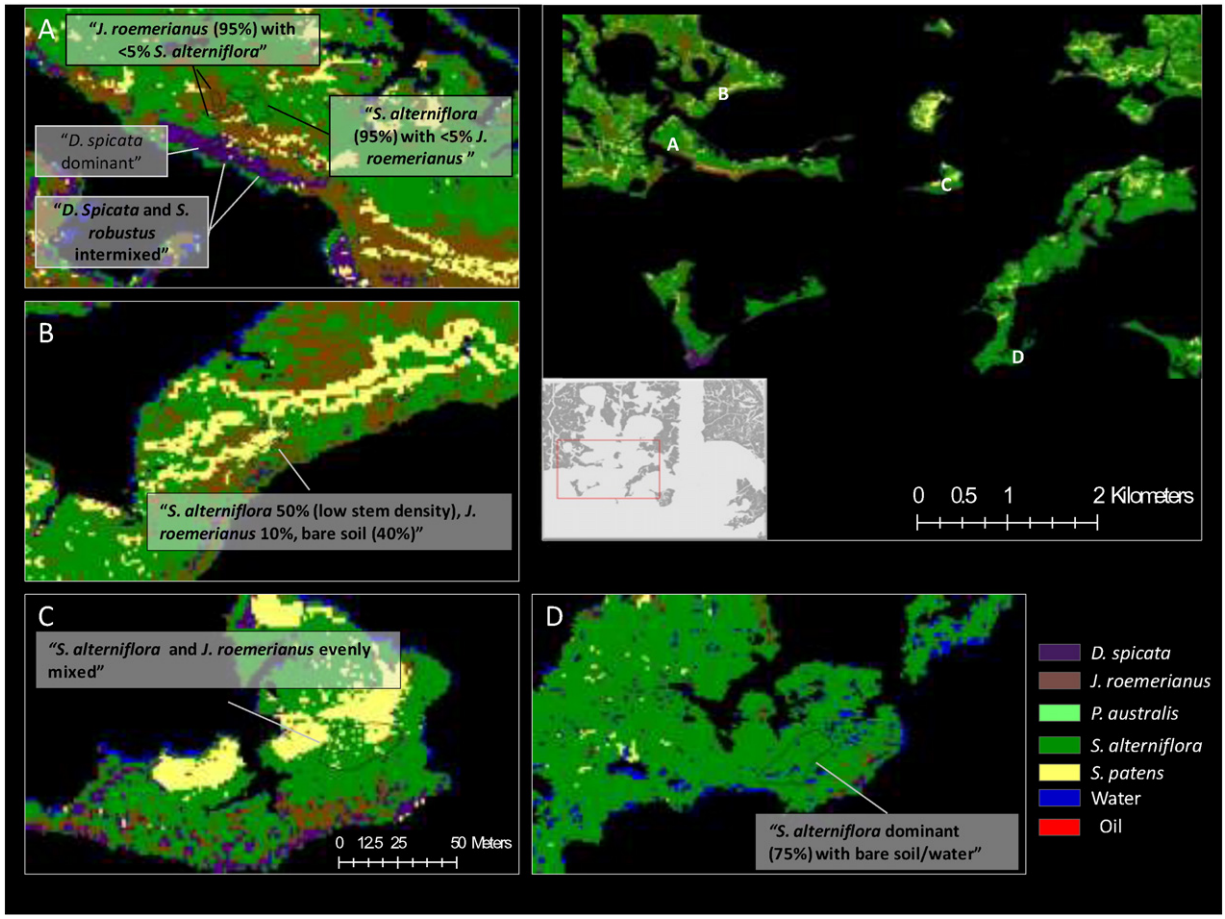

Fig. 9. Classification map of dominant species in October 2011. Expanded view boxes A and D show areas with validation polygons where the CDA classifier performed well, and expanded view boxes B and C show areas of poor classification results.

In contrast to stability at some sites (2 and 3), site 4 exhibited heavy vegetation damage and shoreline erosion following the oiling and additional disturbance caused by Hurricane Isaac in August 2012 (Figs. 8& 9B). A comparison of the reported observations and our classified maps indicate we successfully captured the land-cover change documented in this marsh location. The marsh shoreline retreated 27 to 31 m along these transects, and our classifications reflect this shoreline loss (Fig. 8). The most remarkable changes at site 4 (and along other shorelines) occurred between 2011 and 2012, as the open water intruded from the shoreline into the interior marshes by >30 m in some locations (Fig. 8). The shoreline change is more complicated than shoreline retreat. The shoreline change appears to be a function of retreat plus the formation of new tidal channels and mudflats in the near-shore marsh interior, perhaps developed following the storm surge from Hurricane Isaac (Figs. 8& 9B.

The most striking result from the times series analysis is the decrease in overall marsh area in the oiled shoreline zones. Fig. 10B illustrates the transition from oiled marsh to subtidal, open water over the period of the study. Our examination of a subset of generally south-facing (i.e. 70° to 270°) shorelines that are bifurcated into oiled and non-oiled locations indicate that both shoreline zones exhibited retreat, however, oiled marshes loss appreciably more area (Table 3B & C). We found an 8% (~15,351 m^2) greater decrease in total marsh area for oiled shoreline zones (−12%) than for non-oiled shoreline zones (−6%) from 2010 to 2012 suggesting that, in comparison to similarly situated marsh shorelines, oil contamination exacerbated marsh area loss. Furthermore, the results point to the potential vulnerability of shorelines lacking vegetated soil stability to storms that are common in the region.

Tidal stage is widely known to influence vegetation reflectance characteristics and estimates of wetland area, resulting in classification and change detection assessment uncertainty (Jensen et al., 1993; Dobson et al., 1995; Kearney et al., 2009). We anticipated *S. alterniflora* and *P. australis* to have the near-infrared reflectance similar to that of the "pure" GV spectra shown in Fig. 4, due to the leaf structure (i.e. high leaf area) of these species, and *P. australis* exhibits comparable reflectance in this region. Yet, *S. alterniflora* reflectance is much lower than expected, which could be attributable to the influence of background water, resulting from a relatively high tidal stage during the AVIRIS collection period in 2010 (0.246–0.138 m above MLLW).

The percent loss of wetlands in oiled zones (12%, 173,799 m^2) is likely an underestimate of the actual loss, due to the offset caused by lower water levels in 2011 and 2012 compared with the base image (2010). The maximum tidal difference between data capture periods (2010 and 2011) is 22 cm, and a minimum difference of 4 cm from low tide in 2010 to high tide in 2012. In determining the effect of tidal stage on remotely sensed classification/change detection products in *S. alterniflora* dominated marshes of South Carolina, Jensen et al. (1993) found that for every 10 cm of water level change wetland area changed by 1–2%. Using this metric, a 22 cm decrease in water level (maximum difference during data capture periods) could increase wetland loss in oiled zones as much as 4% (43,955 m^2). However, a great deal of uncertainty lies in predicting the impacts of water level on wetland area change estimates.

The salt marshes where the heaviest oiling occurred were dominated by *S. alterniflora* and *J. roemerianus*, but only *S. alterniflora* were extensively degraded or lost in the oiled zones (Table 3B). The relative even distribution of *J. roemerianus* from 2010 to 2012 (10–12%) suggest

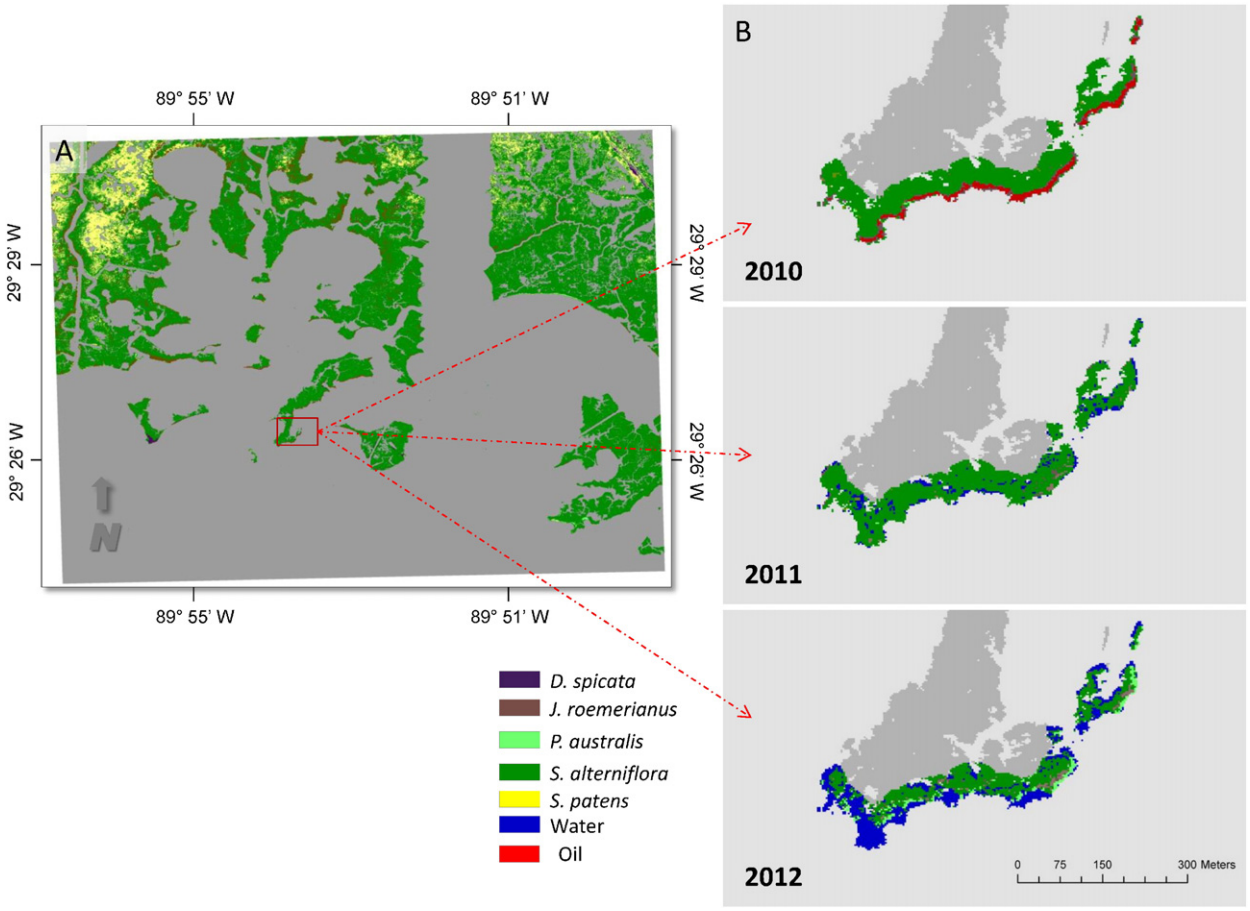

Fig. 10. A) Map of dominant species in 2010. The shorelines in the north were among the most heavily oiled marshes following the DWH spill. B) Progression of marsh loss from 2010 to 2012 on a heavily oiled shoreline.

that *J. roemerianus* was less sensitive to oiling than *S. alterniflora*. This assertion contradicts field and greenhouse mesocosm experiments which have shown *S. alterniflora* to have a higher tolerance threshold for oil contamination (Lin et al., 2002, Lin and Mendelssohn, 2012). An alternative explanation is that the disproportional negative response of *S. alterniflora* is due to its spatial distribution and landscape position. For example, *J. roemerianus* commonly dominates intermediate marsh zones and is not as widely spread on the shoreline edge, or on the southern, bayside islands that are closest to the Gulf of Mexico (Fig. 6). Conversely, *S. alterniflora* is widespread on the marsh shoreline edges of these islands, which suggests that *S. alterniflora* marshes may be more vulnerable to wave action and storm surge erosion following oiling, due to their landscape position (Fig. 6).

Our results showing variable marsh responses to heavy oiling are supported by previous field observations (Lin and Mendelssohn, 2012; Silliman et al., 2012). Silliman et al. (2012) highlighted the importance of landscape position and biogeomorphological feedbacks in the variable responses of marsh ecosystems to disturbance, and that heavily oiled shorelines amplified erosion in areas already experiencing elevated rates of retreat, due to multiple human stressors. Erosion rates along heavily oiled shorelines of already receding platforms were more than twice that of reference sites one-and-a-half years after the spill began. Conversely, shoreline erosion was suppressed at heavily oiled sites with different geomorphic and/or vegetation properties as these sites showed evidence of recovery with plant cover meeting or exceeding that of reference sites through lateral (clonal) regrowth originating from the marsh interior (Silliman et al., 2012). More recently, Zengel et al. (2015) has indicated that manual oil treatments (i.e. oil and oiled debris removal) conducted by small crews improved habitat conditions by exposing residual oiling to natural degradation processes and minimizing additional detrimental effects (Zengel et al., 2015). Furthermore, *S. alterniflora* planting, following treatment, increased vegetation recovery and reduced shoreline erosion (Zengel et al., 2015). Going forward, marsh shoreline change should be further examined, with consideration of different treatment and re-vegetation methods, using imaging spectroscopy.

5. Conclusion

We demonstrated the capacity of a time series of airborne imaging spectroscopic data (AVIRIS) to distinguish spectrally similar plant species in a salt marsh ecosystem heavily impacted by oil. We used canonical discriminant analysis (CDA) to classify dominant species, and verified distributions with temporally corresponding field data. Finally, we compared changes in dominant species percent cover during three years (October 2010, 2011 and 2012) along oiled and non-oiled shorelines with comparable locations, inshore distance and orientation.

S. alterniflora was by far the most widespread dominant in oiled zones. *J. roemerianus* and *S. patens* were common dominants, but were not frequently dominant in the southern portion of the study area that was most impacted by oil. *D. spicata* was a pioneer species following oiling disturbance. Both oiled and non-oiled shorelines showed signs of shoreline erosion, but oiled shorelines exhibited more than twice as much loss 2.5 years after initial oiling. Damage to vegetation from oil may have increased the vulnerability of the shoreline to erosion during subsequent extreme events. Marshes that were heavily oiled exhibited variable degrees of loss and recovery, suggesting other factors may have contributed to the marsh responses.

Future research will build upon the findings here by analyzing marsh transitions following oiling using sub-pixel mixture modeling

techniques, and determine whether observed marsh responses (i.e. recovery, type-conversion, degradation, or loss) are functions of oil distribution (oil EM fractions, oil penetration and persistence) and/or tidal and wave height properties. The goal is to improve predictions of marsh ecosystem responses (i.e. degradation and resiliency), and in doing so, advance mitigation and management efforts.

Acknowledgments

We thank the NASA AVIRIS team for their efforts in collecting and preprocessing the large volume of data that made this and other post-spill studies possible. Gregg Swayze and Greg Steyer of the U.S. Geological Survey (USGS) for their contribution in field spectroscopy data collection. Brett Patton, Michael Bell, Brady Couvillion and the USGS team for their assistance in locating sampling sites, species identification and for supplying the survey data used in map validation. This research was partially supported by a NSF grant (NSF RAPID grant # 1058134 "Analysis of NASA's Advanced Visible Infrared Imaging Spectrometer data acquired over multiple dates and flightlines along the northern Gulf coastline, including barrier islands," Principal Investigator S. Ustin) and by a NASA Earth and Space Sciences Fellowship (13-EARTH13F-0052).

Any use of trade, product, or firm names is for descriptive purposes only and does not imply endorsement by the U.S. Government.

References

Adam, E., Mutanga, O., & Rugege, D. (2010). Multispectral and hyperspectral remote sensing for identification and mapping of wetland vegetation: A review. *Wetlands Ecology and Management*, *18*(3), 281–296.

Alexander, S. K., & Webb, J. W., Jr. (1985). Oil in the salt marsh: what have we learned. *Proceedings, Fourth Coastal Marsh and Estuary Management Symposium* (pp. 49–62). Baton Rouge, LA: Louisiana State University Printing Office.

Allen, Y. C., Couvillion, B. R., & Barras, J. A. (2012). Using multitemporal remote sensing imagery and inundation measures to improve land change estimates in coastal wetlands. *Estuaries and Coasts*, *35*(1), 190–200.

Alonzo, M., Roth, K., & Roberts, D. (2013). Identifying Santa Barbara's urban tree species from AVIRIS imagery using canonical discriminant analysis. *Remote Sensing Letters*, *4*(5), 513–521.

Asner, G. P. (1998). Biophysical and biochemical sources of variability in canopy reflectance. *Remote Sensing of Environment*, *64*(3), 234–253.

Asner, G. P., Borghi, C. E., & Ojeda, R. A. (2003). Desertification in Central Argentina: Changes in ecosystem carbon and nitrogen from imaging spectroscopy. *Ecological Applications*, *13*, 629–648.

Boardman, J. W. (1999). February). *Precision geocoding of low altitude AVIRIS data: lessons learned in, 1998* (In AVIRIS 1999 Proceedings).

Ceccato, P., Flasse, S., Tarantola, S., Jacquemoud, S., & Gregoire, J. -M. (2001). Detecting vegetation leaf water content using reflectance in the optical domain. *Remote Sensing of Environment*, *77*, 22–33.

Chabreck, R. H. (1972). *Vegetation, water and soil characteristics of the Louisiana coastal Louisiana State UniversityAgricultural Experiment Station Bulletin No. 664.* Baton Rouge, Louisiana: Louisiana State University.

Chen, D., & Stow, D. (2002). The effect of training strategies on supervised classification at different spatial resolutions. *Photogrammetric Engineering and Remote Sensing*, *68*(11), 1155–1162.

Clark, R. N., Swayze, G. A., Livo, K. E., Kokaly, R. F., King, T. V. V., Dalton, J. B., ... McDougal, R. R. (2002). Surface reflectance calibration of terrestrial imaging spectroscopy data. In Green R.O. (Ed.), *Proceedings of the eleventh JPL airborne earth science workshop. 03–04.* (pp. 43–64). JPL Publication.

Clewell, A. F., Beaman, R. S., Coultas, C. L., & Lasley, M. E. (1999). *Suwannee River tidal marsh vegetation and its response to external variables and endogenous community processes.* Live Oak, FL: Final Report. Report prepared for the Suwannee River Water Management District (119 pp).

Couvillion, B. R., Barras, J. A., Steyer, G. D., Sleavin, W., Fischer, M., Beck, H., ... Heckman, D. (2011). *Land area change in coastal Louisiana from 1932 to 2010: U.S. Geological Survey Scientific Investigations Map 3164, scale 1:265,000,.* (12 p. pamphlet).

DeLaune, R. D., Pezeshki, S. R., Jugsujinda, A., & Lindau, C. W. (2003). Sensitivity of US Gulf of Mexico coastal marsh vegetation to crude oil: Comparison of greenhouse and field responses. *Aquatic Ecology*, *37*(4), 351–360.

Demmig-Adams, B., & Adams, W. W. (1996). The role of xanthophyll cycle carotenoids in the protection of photosynthesis. *Trends in Plant Science*, *1*(1), 21–26.

Dennison, Philip E., & Roberts, D. A. (2003). Endmember selection for multiple endmember spectral mixture analysis using endmember average RSME. *Remote Sensing of Environment*, *87*(2–3), 123–135.

Dobson, J. E., Bright, E. A., Ferguson, R. L., Field, D. W., Wood, L. L., Haddad, K. D., ... Thomas, J. P. (1995). *NOAA Coastal Change Analysis Program (C-CAP): Guidance for Regional Implementation. NOAA Technical Report NMFS 123, NOAA NMFS.* (Seattle, Washington, 92 p).

Dópido, I., Villa, A., Plaza, A., & Gamba, P. (2012). A quantitative and comparative assessment of unmixing-based feature extraction techniques for hyperspectral image classification. *IEEE J. Sel. Topics Applied Earth Observations and Remote Sens.*, *5*(2), 421–435.

Feret, J. -B., Francois, C., Asner, G. P., Gitelson, A. A., Martin, R. E., Bidel, L. P. R., ... Jacquemoud, S. (2008). PROSPECT-4 and 5: Advances in the leaf optical properties model separating photosynthetic pigments. *Remote Sensing of Environment*, *112*(6), 3030–3043.

Fisher, R. A. (1936). The use of multiple measurements in taxonomic problems. *Annals of Eugenics*, *7*(2), 179–188.

Foody, G. M., McCulloch, M. B., & Yates, W. B. (1995). Classification of remotely sensed data by an artificial neural network: Issues related to training data characteristics. *Photogrammetric Engineering and Remote Sensing*, *61*(4), 391–401.

Frieswyk, C. B., Johnston, C. A., & Zedler, J. B. (2007). Identifying and characterizing dominant plants as an indicator of community condition. *Journal of Great Lakes Research*, *33*(sp3), 125–135.

Gamon, J. A., Serrano, L., & Surfus, J. S. (1997). The photochemical reflectance index: An optical indicator of photosynthetic radiation-use efficiency across species, functional types, and nutrient levels. *Oecologia*, *112*, 492–501.

Gosselink, J., & Pendleton, E. C. (1984). *The ecology of delta marshes of coastal Louisiana: a community profile.* Center for Wetland Resources: Louisiana State University, Baton Rouge.

Green, R. O., Eastwood, M. L., Sarture, C. M., Chrien, T. G., Aronsson, M., Chippendale, B. J., ... Williams, O. (1998). Imaging spectroscopy and the airborne visible/infrared imaging spectrometer (AVIRIS). *Remote Sensing of Environment*, *65*(3), 227–248.

Guang, Z., & Maclean, A. L. (2000). A comparison of canonical discriminant analysis and principal component analysis for spectral transformation. *PE&RS, Photogrammetric Engineering & Remote Sensing*, *66*(7), 841–847.

Halligan, K. Q. (2002). *Multiple endmember spectral mixture analysis of vegetation in the northeast corner of Yellowstone national park.* Master's Thesis: University of California Santa Barbara.

Hester, M. W., & Mendelssohn, I. A. (2000). Long-term recovery of a Louisiana brackish marsh plant community from oil-spill impact: Vegetation response and mitigating effects of marsh surface elevation. *Marine Environmental Research*, *49*(3), 233–254.

Hopkinson, C. S., Gosselink, J. G., & Parrando, R. T. (1978). Aboveground production of seven marsh plant species in coastal Louisiana. *Ecology*, 760–769.

Hughes, G. (1968). On the mean accuracy of statistical pattern recognizers. *Information Theory, IEEE Transactions on*, *14*(1), 55–63.

Jensen, J. R., Cowen, D. J., Althausen, J. D., Narumalani, S., & Weatherbee, O. (1993). The detection and prediction of sea level changes on coastal wetlands using satellite imagery and a geographic information system. *Geocarto International*, *8*(4), 87–98.

Judd, C., Steinberg, S., Shaughnessy, F., & Crawford, G. (2007). Mapping salt marsh vegetation using aerial hyperspectral imagery and linear unmixing in Humboldt Bay, California. *Wetlands*, *27*(4), 1144–1152.

Kearney, M. S., Stutzer, D., Turpie, K., & Stevenson, J. C. (2009). The effects of tidal inundation on the reflectance characteristics of coastal marsh vegetation. *Journal of Coastal Research*, 1177–1186.

Khanna, S., Santos, M. J., Ustin, S. L., Koltunov, A., Kokaly, R. F., & Roberts, D. A. (2013). Detection of salt marsh vegetation stress and recovery after the Deepwater horizon oil spill in Barataria bay, Gulf of Mexico using AVIRIS data. *PloS One*, *8*(11), e78989.

Kirby, C. J., & Gosselink, J. G. (1976). Primary production in a Louisiana Gulf Coast *S. alterniflora* marsh. *Ecology*, 1052–1059.

Kokaly, R. F., Asner, G. P., Ollinger, S. V., Martin, M. E., & Wessman, C. A. (2009). Characterizing canopy biochemistry from imaging spectroscopy and its application to ecosystem studies. *Remote Sensing of Environment*, *113*, S78–S91.

Kokaly, R. F., Couvillion, B. R., Holloway, J. M., Roberts, D. A., Ustin, S. L., Peterson, S. H., ... Piazza, S. C. (2013). Spectroscopic remote sensing of the distribution and persistence of oil from the Deepwater Horizon spill in Barataria Bay marshes. *Remote Sensing of Environment*, *129*, 210–230.

Kühn, F., Oppermann, K., & Hörig, B. (2004). Hydrocarbon index–an algorithm for hyperspectral detection of hydrocarbons. *International Journal of Remote Sensing*, *25*(12), 2467–2473.

Lehr, B., Nristol, S., & Possolo, A. (2010). *Oil budget calculator—Deepwater horizon, technical documentation: A report to the National Incident Command.* Cent: Coastal Response Res.

Levine, J. M., Brewer, J. S., & Bertness, M. D. (1998). Nutrients, competition and plant zonation in a New England salt marsh. *Journal of Ecology*, *86*(2), 285–292.

Lin, Q., & Mendelssohn, I. A. (1996). A comparative investigation of the effects of South Louisiana crude oil on the vegetation of fresh, brackish and salt marshes. *Marine Pollution Bulletin*, *32*(2), 202–209.

Lin, Q., & Mendelssohn, I. A. (2012). Impacts and recovery of the Deepwater Horizon oil spill on vegetation structure and function of coastal salt marshes in the northern Gulf of Mexico. *Environmental Science & Technology*, *46*(7), 3737–3743.

Lin, Q., Mendelssohn, I. A., Suidan, M. T., Lee, K., & Venosa, A. D. (2002). The dose-response relationship between No. 2 fuel oil and the growth of the salt marsh grass, Spartina alterniflora. *Marine Pollution Bulletin*, *44*(9), 897–902.

Lu, D., & Weng, Q. (2007). A survey of image classification methods and techniques for improving classification performance. *International Journal of Remote Sensing*, *28*(5), 823–870.

Mendelssohn, I. A., Hester, M. W., Sasser, C., & Fischel, M. (1990). The effect of a Louisiana crude oil discharge from a pipeline break on the vegetation of a southeast Louisiana brackish marsh. *Oil and Chemical Pollution*, *7*(1), 1–15.

Michel, J., Owens, E. H., Zengel, S., Graham, A., Nixon, Z., Allard, T., ... Taylor, E. (2013). Extent and degree of shoreline oiling: Deepwater Horizon oil spill, Gulf of Mexico, USA. *PloS One*, *8*(6), e65087.

Mitsch, W. J., & Gosselink, J. G. (2000). *Wetlands* (3rd ed.). New York: John Wiley.

Moore, P. D., & Chapman, S. B. (1986). *Methods in plant ecology*. Oxford: Blackwell Scientific Publications.

Morris, J. T., & Haskin, B. (1990). A 5-yr record of aerial primary production and stand characteristics of *S. alterniflora*. *Ecology*, 2209–2217.

Nagler, P. L., Inoue, Y., Glenn, E. P., Russ, A. L., & Daughtry, C. S. T. (2003). Cellulose absorption index (CAI) to quantify mixed soil–plant litter scenes. *Remote Sensing of Environment*, *87*, 310–325.

Palacios-Orueta, A., & Ustin, S. L. (1996). Multivariate statistical classification of soil spectra. *Remote Sensing of Environment*, *57*(2), 108–118.

Penland, S., & Ramsey, K. E. (1990). Relative sea-level rise in Louisiana and the Gulf of Mexico: 1908–1988. *Journal of Coastal Research*, 323–342.

Peterson, S. H., Roberts, D. A., Beland, M., Kokaly, R. F., & Ustin, S. L. (2015). Oil detection in the coastal marshes of Louisiana using MESMA applied to band subsets of AVIRIS data. *Remote Sensing of Environment*, *159*, 222–231.

Pezeshki, S. R., & DeLaune, R. D. (1991). A comparative study of above-ground productivity of dominant US Gulf Coast marsh species. *Journal of Vegetation Science*, *2*(3), 331–338.

Pezeshki, S. R., & De Laune, R. D. (1993). Effect of crude oil on gas exchange functions of *J. roemerianus* and *S. alterniflora*. *Water, Air, and Soil Pollution*, *68*(3–4), 461–468.

Pezeshki, S. R., Hester, M. W., Lin, Q., & Nyman, J. A. (2000). The effects of oil spill and clean-up on dominant US Gulf coast marsh macrophytes: A review. *Environmental Pollution*, *108*(2), 129–139.

Plaza, A., Benediktsson, J. A., Boardman, J. W., Brazile, J., Bruzzone, L., Camps-Valls, G., ... Trianni, G. (2009). Recent advances in techniques for hyperspectral image processing. *Remote Sensing of Environment*, *113*, S110–S122.

Pu, R., & Liu, D. (2011). Segmented canonical discriminant analysis of in situ hyperspectral data for identifying 13 urban tree species. *International Journal of Remote Sensing*, *32*(8), 2207–2226.

Reddy, K. Ramesh, & Delaune, D. Ronald (2008). *Biogeochemistry of wetlands: Science and applications*. Boca Raton, FL: CRC Press, Taylor and Francis Group (757 pp).

Roberts, D. A., Gardner, M., Church, R., Ustin, S., Scheer, G., Roberts Gardner, M., ... Green, R. O. (1998). Mapping chaparral in the Santa Monica Mountains using multiple endmember spectral mixture models. *Remote Sensing of Environment*, *65*(3), 267–279.

Rogan, J., Franklin, J., & Roberts, D. A. (2002). A comparison of methods for monitoring multitemporal vegetation change using thematic mapper imagery. *Remote Sensing of Environment*, *80*(1), 143–156.

Roth, K. L., Dennison, P. E., & Roberts, D. A. (2012). Comparing endmember selection techniques for accurate mapping of plant species and land cover using imaging spectrometer data. *Remote Sensing of Environment*, *127*, 139–152 (null).

Roth, K. L., Roberts, D. A., Dennison, P. E., Alonzo, M., Peterson, S. H., & Beland, M. (2015). Differentiating plant species within and across diverse ecosystems with imaging spectroscopy. *Remote Sensing of Environment*, *167*, 135–151.

Sadro, S., Gastil-Buhl, M., & Melack, J. (2007). Characterizing patterns of plant distribution in a southern California salt marsh using remotely sensed topographic and hyperspectral data and local tidal fluctuations. *Remote Sensing of Environment*, *110*(2), 226–239.

Sasser, C. E., Visser, J. M., Mouton, Edmond, Linscombe, Jeb, & Hartley, S. B. (2008). *Vegetation types in coastal Louisiana in 2007: U.S. Geological Survey Open-File Report 2008–1224*. (1 sheet, scale 1:550,000).

Schmidt, K. S., & Skidmore, A. K. (2003). Spectral discrimination of vegetation types in a coastal wetland. *Remote Sensing of Environment*, *85*(1), 92–108.

Schmidt, K. S., Skidmore, A. K., Kloosterman, E. H., Van Oosten, H., Kumar, L., & Janssen, J. A. M. (2004). Mapping coastal vegetation using an expert system and hyperspectral imagery. *Photogrammetric Engineering & Remote Sensing*, *70*(6), 703–715.

Serrano, L., Penuelas, J., & Ustin, S. L. (2002). Remote sensing of nitrogen and lignin in Mediterranean vegetation from AVIRIS data: Decomposing biochemical from structural signals. *Remote Sensing of Environment*, *81*, 355–364.

Silliman, B. R., Van de Koppel, J., McCoy, M. W., Diller, J., Kasozi, G. N., Earl, K., Adams, P. N., et al. (2012). Degradation and resilience in Louisiana salt marshes after the BP–Deepwater Horizon oil spill. *Proceedings of the National Academy of Sciences*, *109*(28), 11234–11239.

Somers, B., Asner, G. P., Tits, L., & Coppin, P. (2011). Endmember variability in spectral mixture analysis: A review. *Remote Sensing of Environment*, *115*(7), 1603–1616.

Somers, B., Delalieux, S., Stuckens, J., Verstraeten, W. W., & Coppin, P. (2009). A weighted linear spectral mixture analysis approach to address endmember variability in agricultural production systems. *International Journal of Remote Sensing*, *30*, 139–147.

Somers, B., Delalieux, S., Verstraeten, W. W., Van Aardt, J. A. N., Albrigo, G. L., & Coppin, P. (2010). An automated waveband selection technique for optimized hyperspectral mixture analysis. *International Journal of Remote Sensing*, *31*(20), 5549–5568.

Stedman, S., & Dahl, T. E. (2008). *Status and trends of wetlands in the coastal watersheds of the Eastern United States 1998 to 2004. National Oceanic and Atmospheric Administration*. Fish and Wildlife Service: National Marine Fisheries Service and U.S. Department of the Interior.

Shumway, S. W. (1995). Physiological integration among clonal ramets during invasion of disturbance patches in a New England salt marsh. *Annals of Botany*, *76*(3), 225–233.

Ustin, S. L., & Gamon, J. A. (2010). Remote sensing of plant functional types. *New Phytologist*, *186*(4), 795–816.

Ustin, S. L., Gitelson, A. A., Jacquemoud, S., Schaepman, M., Asner, G. P., Gamon, J. A., & Zarco-Tejada, P. J. (2009). Retrieval of foliar information about plant pigment systems from high resolution spectroscopy. *Remote Sensing of Environment*, *113*, 67–77.

Visser, J. M., Sasser, C. E., Chabreck, R. H., & Linscombe, R. G. (1998). Marsh vegetation types of the Mississippi River deltaic plain. *Estuaries*, *21*(4), 818–828.

Xie, Yichun, Sha, Zongyao, & Yu, Mei (2008). Remote sensing imagery in vegetation mapping: A review. *Journal of Plant Ecology (2008)*, *1*(1), 9–23.

Zengel, S., Bernik, B. M., Rutherford, N., Nixon, Z., & Michel, J. (2015). Heavily oiled salt marsh following the Deepwater Horizon oil spill, ecological comparisons of shoreline cleanup treatments and recovery. *PloS One*, *10*(7), e0132324.